Marine Structures 78 (2021) 102979

Contents lists available at ScienceDirect

Marine Structures

journal homepage: http://www.elsevier.com/locate/marstruc

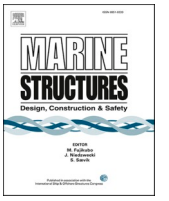

An object-oriented method for fully coupled analysis of floating offshore wind turbines through mapping of aerodynamic coefficients

Omar El Beshbichi *, Yihan Xing, Muk Chen Ong

Department of Mechanical and Structural Engineering and Materials Science, University of Stavanger, Stavanger, Norway

ARTICLE INFO

Keywords:
Fully-coupled analysis
Steady-state aerodynamics
Modelica
Floating offshore wind turbines
OC3 phase IV
Spar-buoy

ABSTRACT

This work presents a novel object-oriented approach to model the fully-coupled dynamic response of floating offshore wind turbines (FOWTs). The key features offered by the method are the following: 1) its structure naturally allows for easy implementation of arbitrary platform geometries and platform/rotor configurations, 2) the analysis time is significantly faster than that of standard codes and results are accurate in situations where rotor dynamic contribution is negligible, and 3) an extremely flexible modeling environment is offered by the object-oriented nature of Modelica. Moreover, the current modeling facility used for the code development is open source and is naturally suitable for code sharing. In the present method, the aerodynamic model computes the aerodynamic loads through the mapping of steady-state aerodynamic coefficients. This modeling approach can be placed at the intersection between simplified aerodynamic methods, such as TDHMill, and full beam element/momentum-based aerodynamic methods. Aerodynamic loads obtained from the coefficients mapping are composed of a concentrated thrust and a concentrated torque. The thrust acts at the hub, while the torque is applied at the rotor low-speed shaft of a simplified rigid rotor equation of motion (EoM) used to emulate the rotor response. The aerodynamic coefficients are computed in FAST for a baseline 5 MW wind turbine. A standard rotor-collective blade-pitch control model is implemented. The system is assumed to be rigid. Linear hydrodynamics is employed to compute hydrodynamic loads. The industry-standard numerical-panel code Sesam-Wadam (DNV-GL) is used to preprocess the frequency-domain hydrodynamic problem. Validation of the code considers a standard spar-buoy platform, based on the Offshore Code Comparison Collaboration (OC3-Hywind). The dynamic response is tested in terms of free-decay response, Response Amplitude Operator (RAO), and the time histories and power spectral densities (PSDs) of several load cases including irregular waves and turbulent wind. The resulting model is benchmarked against well-known code-to-code comparisons and a good agreement is obtained.

1. Introduction

Commercial deployment of FOWTs is still at an early stage, while several FOWTs research prototypes have been deployed in the recent past. Examples are the Hywind Demo, 2.3 MW FOWT developed by Equinor ASA and deployed in Karmy, Norway in 2009 [1],

* Corresponding author.
E-mail address: omar.elbeshbichi@uis.no (O. El Beshbichi).

https://doi.org/10.1016/j.marstruc.2021.102979
Received 14 September 2020; Received in revised form 2 February 2021; Accepted 20 February 2021
Available online 6 March 2021

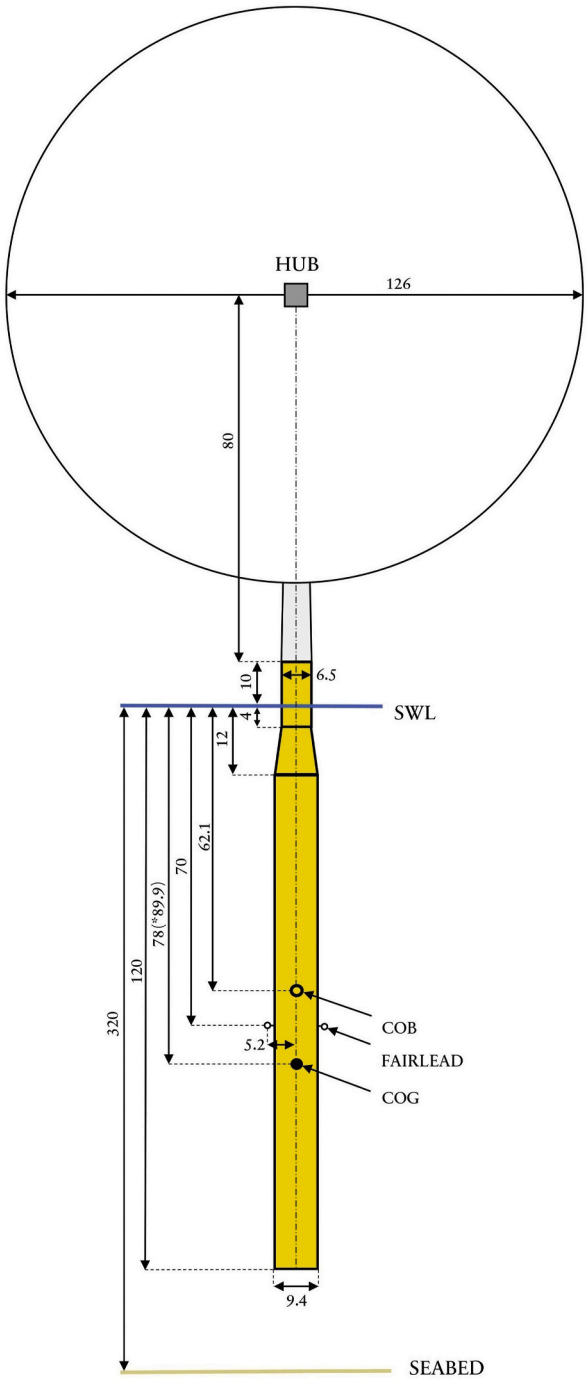

Fig. 1. OC3-Hywind Geometry [m] (* COG is 89.9 m when only the OC3 platform is considered).

and WindFloat®, 2 MW FOWT prototype developed by Principle Power, Inc. and deployed in Aguadoura, Portugal in 2011 [2]. As of 2018, the only commercial floating wind farm in operation is Hywind Scotland, developed by Equinor ASA and deployed off the coast of Peterhead, Scotland [3].

The installation of offshore wind turbines currently relies on fixed foundations, of which three major classes are monopile, jacket, and tripod [4]. The major limitation of these designs is the maximum water depth at which they are economically feasible to deploy. The maximum water depth at which they can be used is set to approximately 50 m (shallow water sites), while the average water depth of currently deployed wind farms is 27.2 m [4]. However, most of the ideal offshore wind energy sites across the globe are characterized by much deeper water depths [5]. In deep water, FOWTs may be economically favourable with respect to wind turbines

Table 1
OC3-hywind spar-buoy platform specifications [5,13,14].

Water Depth	m	320
Water Density	kg/m^3	1025
Drag Coefficient	–	0.6
Diameter	m	6.5 to 9.4 (tapered)
Draft	m	120
Water Displacement	m^3	8029
Mass (including ballast)	kg	$7.4x10^6$
Depth to COG	m	89.92
Roll Moment of Inertia about COG	kgm^2	$4.2x10^9$
Pitch Moment of Inertia about COG	kgm^2	$4.2x10^9$
Yaw Moment of Inertia about Centerline	kgm^2	$1.6x10^8$
Number of mooring lines	–	3
Angular distance between adjacent mooring lines	°	120
Unstretched line length	m	902.2
Static mooring line horizontal length	m	848.67
Radius to fairleads	m	5.2
Depth to fairleads	m	70
Line diameter	m	0.09
Line mass density	kg/m	77.71
Mooring Line Weight in Water	N/m	698.09
Mooring Line Extensional Stiffness	N	$3.8x10^8$
Yaw Spring Mooring Stiffness	Nm/rad	$9.8x10^7$

installed on bottom-fixed foundations, and may, therefore, make the exploitation of deep water sites economically more attractive [4,5]. Classification of floating foundations considers the way the structure achieves hydrostatic stability. There are three main floating platform families: the spar-buoy type, the tension leg (TLP) type, and the barge type. In order to achieve stability, spar-buoy platforms use ballast, TLPs use tensioned mooring lines, and barge platforms use the platform water plane static stability [6].

FOWTs are complex multi-domain dynamic systems. Environmental loads associated with wind, waves, and current make fully-coupled dynamic analyses already necessary during conceptual design. In order to predict the dynamic response of new concepts, numerical tools are normally employed. In order to obtain sufficiently accurate predictions, it is necessary to include an accurate account of the hydrodynamic and aerodynamic loads acting on the system, the servo-control system dynamics, and the structural dynamics of the system. This method is called the aero-hydro-elastic-servo fully-coupled approach [4]. However, detailed fully-coupled tools are in general time-consuming. In situations where only the overall dynamic response of the system in operational conditions is needed, such as pre-engineering and conceptual analysis of novel multiple rotor/platform configurations, simplified methods that offer high computational efficiency while providing enough accuracy are appealing.

In this work, the aerodynamic loads are computed by mapping the steady-state aerodynamic coefficients of a baseline 5 MW wind turbine. The aerodynamic coefficients are preventively computed in FAST. An aerodynamic model that considers only simplified rigid rotor dynamics is used to determine the aerodynamic state of the system. The concentrated aerodynamic thrust is applied at the hub, while the concentrated aerodynamic torque is applied at the rotor low-speed shaft. A complete proportional-integrative (PI) controller is implemented in order to compute the rotor-collective blade-pitch angle from the generator speed feedback signal. This method presents itself as a viable alternative to more complex beam element/momentum (BEM) models or overly simplified approaches.

In this work, a simplified fully-coupled method for the dynamic analysis of FOWTs by means of the object-oriented modeling language Modelica is developed. The code is developed in the open-source environment OpenModelica. The development of numerical tools for the analysis of FOWTs written in Modelica is relatively new, albeit sporadic modeling experience exists [7–9]. Modelica is a non-proprietary, object-oriented, equation-based language developed by the non-profit Modelica Association and used to conveniently model complex physical systems [10]. Modelica offers a freely-available *Modelica Standard Library* (MSL), suitable to model dynamic systems of various physical domains, such as mechanical, thermal, control, and electrical. The object-oriented nature of Modelica allows for a flexible way of generating complex multi-domain models and facilitates the reuse of common classes throughout the model. Object-oriented modeling is then convenient when a fully-coupled approach is needed. Modelica language is, therefore, advantageous for the establishment of analysis platforms suitable to be further extended in time by different developers, it greatly aids debugging stages, and it is well suitable for code sharing. Moreover, equation-based modeling does not need the explicit specification of the integration logical flow (acausal modeling). Front-end platforms include commercial and open-source options. Dymola is a common commercial platform, developed by the European company Dassault Systmes and available within CATIA [11]. OpenModelica is the major open-source Modelica platform, mainly used in academic research and supported by the Open Source Modelica Consortium (OSMC) [12].

A code-to-code comparison of responses of the standard OC3-Hywind design is carried out by considering fully-coupled codes commonly used in design practice. The results show how the novel method implemented with Modelica can cover most of the dynamic response of the system within operational conditions. Details regarding the code will be given in the following sections.

Table 2
Total System Inertia Specifications (OC3-Hywind platform, ballast, tower, nacelle, rotor) [5,13,14].

Mass	kg	$8.2x10^6$
Depth to COG	m	78
Roll Moment of Inertia about COG	kgm^2	$1.8x10^{10}$
Pitch Moment of Inertia about COG	kgm^2	$1.8x10^{10}$
Yaw Moment of Inertia about Centerline	kgm^2	$1.9x10^8$

Table 3
OC3-hywind hydrostatic properties [13,15].

Heave Hydrostatic restoring stiffness	N/m	$3.3x10^5$
Roll Hydrostatic restoring stiffness	Nm/rad	$1.3x10^9$
Pitch Hydrostatic restoring stiffness	Nm/rad	$1.3x10^9$
Surge added linear damping	$N/(m/s)$	$1x10^5$
Sway added linear damping	$N/(m/s)$	$1x10^5$
Heave added linear damping	$N/(m/s)$	$1.3x10^5$
Yaw added linear damping	$Nm/(rad/s)$	$1.3x10^7$

Table 4
NREL offshore 5-MW Baseline Wind Turbine Specifications [5].

Rotor Diameter	m	126
Hub Height	m	90
Rotor Mass	kg	$110x10^3$
Nacelle Mass	kg	$240x10^3$
Tower Mass	kg	$347.46x10^3$
Cut-In, Rated, Cut-Out Wind Speed	m/s	3, 11.4, 25
Cut-In, Rated Rotor Speed	rpm	6.9, 12.1

2. System specifications

2.1. OC3-hywind platform

The implementation process is carried through by considering as specific floating platform the standard OC3-Hywind Phase IV spar-buoy design [13]. The reason for choosing the OC3 design is mainly related to the fact that it has been widely studied over the years, and data for code-to-code comparison and quality checks are plenty in literature. Fig. 1 shows the baseline OC3-Hywind geometry. COB refers to the center of buoyancy, while COG refers to the center of gravity. The platform top (tower base) emerges 10 m from the sea water level (SWL). A smaller diameter in the SWL region is used in order to reduce the hydrodynamic loads acting on the platform. The distance from SWL to COG is about 89.9 m when only platform and ballast are considered. If the total system is considered (platform, ballast, tower, nacelle, and rotor), the distance from SWL to COG is about 78 m.

Table 1 summarizes the OC3-Hywind platform specifications. Table 2 summarizes the inertia properties of the total system.

Table 3 summarizes the OC3-Hywind platform hydrostatic properties used in the analysis [5,13–15]. Hydrostatic quantities are computed from metacentric height relationships [15]. Typical added linear damping values are used [13].

2.2. NREL offshore 5 MW baseline wind turbine

Wind turbine specifications are based on the NREL offshore 5 MW Baseline Design which is widely used in literature as reference design [5]. The wind turbine has a diameter of 126 m and it is located at the top of the tower. The hub height from the SWL is about 90 m.

Table 4 summarizes the main wind turbine specifications.

3. Linear hydrodynamics

The following method is based on work by Jonkman et al. [6], where validation and benchmark work can be found. Several assumptions are generally accepted in order to simplify the hydrodynamic problem. The body displacements are assumed to be small, which is a valid assumption in most practical cases [5]. Assuming small body displacements is necessary in order to linearize the hydrodynamic problem, take advantage of the superimposition principle, and employ incident wave models such as Airy wave theory

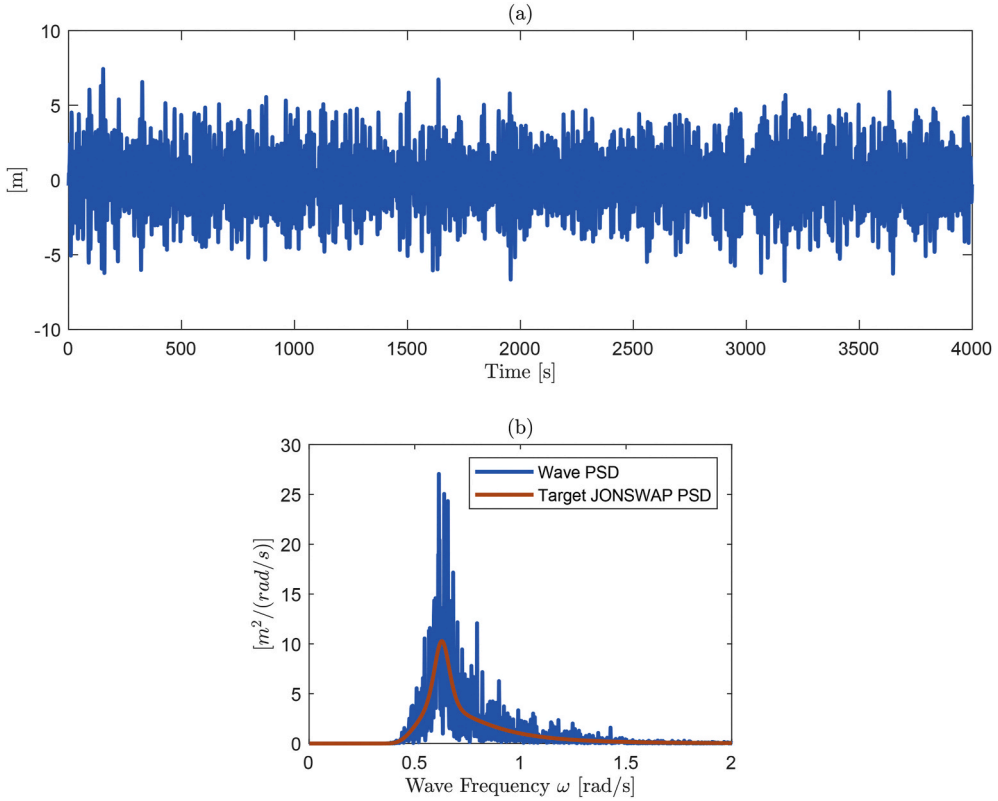

Fig. 2. a) Wave elevation time realization. b) Wave power spectral density computed from time realization versus target JONSWAP power spectral density ($H_s = 6$ m and $T_p = 10$ s).

[15]. The FWT platform is assumed to be a six-degrees of freedom (DOFs) rigid body. The platform dynamics can then be described through six equations of motion, i.e., three translational and three rotational. The linear hydrodynamic problem can be described as follows:

$$[M]\ddot{\underline{q}} + [C]\underline{q} + C_{0,3} = -[A]_{inf}\ddot{\underline{q}} - \int_0^t [K(t-\tau)]\dot{\underline{q}}d\tau + \underline{F}_{waves} + \underline{F}_{mooring} + \underline{F}_{drag} - [B]_{added}\dot{\underline{q}} \tag{1}$$

where $\underline{q}$ is the set of six system DOFs (labelled surge, sway, and heave for the translational DOFs, and roll, pitch, and yaw for the rotational DOFs). $[M]$ is the inertia matrix. $[C]$ is the hydrostatic restoring matrix, generally defined through metacentric height relationships [15]. $C_{0,3}$ is the total buoyancy load from Archimedes' principle ($\rho_{water}V_0 g$, where ρ_{water} is the water density, V_0 is the displaced volume, and g is the gravitational acceleration constant), directed upward in heave direction. $[A]_{inf}$ is the added mass matrix computed at infinite incident wave frequency. The convolution integral term is the wave-radiation potential damping, where [K] is the so-called wave-radiation-retardation kernel matrix. The wave-radiation damping term, together with the added mass term, form the so-called radiation hydrodynamic component. $\underline{F}_{waves}$ are the total dynamic loads from incident waves, $\underline{F}_{mooring}$ are the dynamic loads of the mooring system, $\underline{F}_{drag}$ are the eventual dynamic loads from viscous drag, while $[B]_{added}$ is the eventual linear added damping matrix. In the following sections of this chapter, the major components of the hydrodynamic problem will be discussed in more detail.

3.1. Incident wave loads

The irregular wave elevation, ξ, can be defined as [5]:

$$\xi(t) = \frac{1}{2\pi}\int_{-\infty}^{+\infty} W(\omega)\sqrt{2\pi S^{2-Sided}(\omega)}e^{j\omega t}d\omega \tag{2}$$

Equation (2) is an Inverse Fourier Transform (IFT) of the 2-Sided Wave PSD, $S^{2-Sided}(\omega)$, and results in a time realization. $W(\omega)$ is the Fourier Transform of a White Gaussian Noise (WGN) time realization. $W(\omega)$ can be defined in several ways. In this work, it is defined through the piecewise Box-Muller formulation [16]:

$$\begin{cases} W(\omega) = 0, & \text{if } \omega = 0 \\ W(\omega) = r(cos\varphi + jsin\varphi), & \text{if } \omega > 0 \\ W(\omega) = r(cos\varphi - jsin\varphi), & \text{if } \omega < 0 \end{cases} \tag{3}$$

where:

$$\begin{aligned} r &= \sqrt{-2ln[U_1(|\omega|)]} \\ \varphi &= 2U_2(|\omega|) \end{aligned} \tag{4}$$

where $U_1(\omega)$ and $U_2(\omega)$ are independent random samples defined on the unit interval (0,1).

The 2-Sided Wave PSD is commonly defined by means of the JOint North Sea WAve Project (JONSWAP) spectra, based on the Pierson-Moskowitz spectra. They are defined in the design standard IEC 61400-3 [17].

The incident wave loads time realization, $\underline{F}_{waves}(t)$, is related to the wave elevation and defined as [5]:

$$\underline{F}_{waves}(t) = \frac{1}{2\pi}\int_{-\infty}^{+\infty} W(\omega)\sqrt{2\pi S^{2-Sided}(\omega)}\underline{X}(\omega,\psi)e^{i\omega t}d\omega \tag{5}$$

where ψ is the heading angle, and $\underline{X}(\omega,\psi)$ is the vector of wave-excitation loads on the platform per unit wave amplitude.

Once the procedure for the implementation of irregular incident wave loads is complete, regular waves can be implemented by defining the PSD of a sinusoidal wave of amplitude A and frequency ω^*:

$$\begin{cases} S_r^{1-Sided}(\omega) = 0, & \text{if } \omega \neq \omega^* \\ S_r^{1-Sided}(\omega) = \dfrac{\left(A/\sqrt{2}\right)^2}{d\omega}, & \text{if } \omega = \omega^* \end{cases} \tag{6}$$

where $d\omega$ is the frequency resolution of the PSD in rad/s.

Fig. 2 shows an example of a typical wave amplitude time realization (in this case relative to $H_s = 6$ m and $T_p = 10$ s), together with the comparison between the target JONSWAP PSD and the power spectral density calculated from the time realization. The white gaussian noise contribution is clearly visible.

3.2. Wave-radiation damping

The wave-radiation damping term, $\int_0^t[K(t-\tau)]\underline{\dot{q}}d\tau$, also called potential damping, is a convolution integral implementing memory effects of the platform interacting with the fluid [5]. The convolution representation was first proposed by Cummins [18]. If i and j are DOFs indices, the wave-radiation-retardation kernel $K_{ij}(t)$ represents the hydrodynamic load acting upon the platform in direction i due to a unit platform velocity impulse in direction j. The wave-radiation-retardation kernel matrix is commonly computed by an Inverse Cosine Transform (ICT) time realization of the frequency-domain damping matrix, $[B(\omega)]$:

$$[K(t)] = \frac{2}{\pi}\int_0^{\infty}[B(\omega)]cos(\omega t)d\omega \tag{7}$$

FAST-HydroDyn implements directly the convolution integral in the time-domain [5]. However, the convolution term is inconvenient for simulation and for the analysis and design of motion control systems [19]. Because the convolution is a dynamic linear operator, it can be approximated by a linear ordinary differential equation or state-space model. Kristiansen and Egeland [20] have first proposed such an approach for the approximation of convolution integrals in hydrodynamic modeling. Duarte [21] expanded HydroDyn with a state-space realization of the convolution term, SS-Fitting.

An approximation of the ij convolution term, μ_{ij}

$$\mu_{ij} \simeq \int_0^t K_{ij}(t-\tau)\dot{q}_{ij}d\tau \tag{8}$$

can be in general defined in the state-space form as:

$$\begin{aligned} \dot{\xi}_{ij} &= [\alpha]_{ij}\xi_{ij} + [\lambda]_{ij}\dot{q}_{ij} \\ \mu_{ij} &= [\theta]_{ij}\xi_{ij} + [\gamma]_{ij}\dot{q}_{ij} \end{aligned} \tag{9}$$

where $[\alpha]_{ij}, [\lambda]_{ij}, [\theta]_{ij}, [\gamma]_{ij}$ are the ij state-space matrices, and ξ_{ij} is the ij state vector. The matrices dimensions are, respectively, (mxm), $(mx1)$, $(1xm)$, and $(1x1)$, where m is the state-space approximation order.

After proper matrix assembly, the total state-space approximation can be defined as:

$$\begin{aligned} \underline{\dot{\xi}} &= [\alpha]\underline{\xi} + [\lambda]\underline{\dot{q}} \\ \underline{\mu} &= [\theta]\underline{\xi} + [\gamma]\underline{\dot{q}} \end{aligned} \tag{10}$$

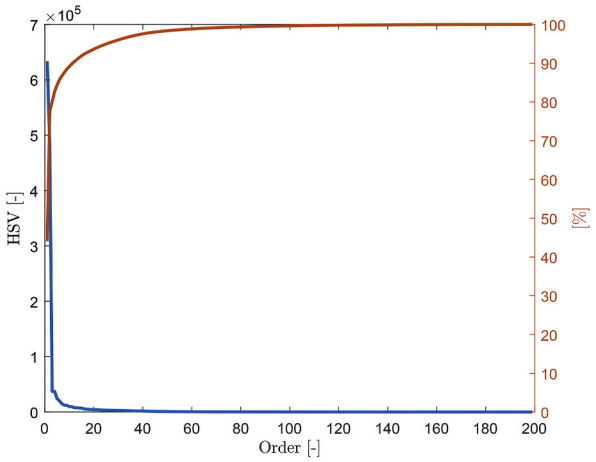

Fig. 3. Hankel Singular Values distribution (HSVs) for the surge-surge wave-radiation-retardation kernel state-space approximation, $K_{11}(t)$.

The final matrices dimensions are, respectively, $(36mx36m)$, $(36mx6)$, $(6x36m)$, and $(6x6)$.

The state-space approximation implementation is typically based on the system identification scheme using the Hankel SVD method, first proposed by Kung [22]. This scheme is implemented in MATLAB in the function IMP2SS (impulse to state-space) in Robust Control Toolbox. If the input unit impulse-response is discrete, the output must be scaled with the time step, dt, according to:

$$\begin{aligned}[\alpha]_{ij} &= [\alpha]_{ij} \\ [\lambda]_{ij} &= [\lambda]_{ij} \\ [\theta]_{ij} &= [\theta]_{ij} dt \\ [\gamma]_{ij} &= 0 \end{aligned} \tag{11}$$

where $[\gamma]_{ij}$ is forced to be zero in order to keep the causality of the system [21].

The method allows for high accuracy but generally employs a very high approximation order ($m > 200$). Consequently, the computational efficiency is reduced [21]. Hankel Singular Values (HSVs) are a measure of the "energy" associated with each state variable of a dynamic system [23]. The HSV distribution of the wave-radiation-retardation kernel state-space approximation follows a Pareto distribution. That is, a small number of states account for most of the total state energy.

Fig. 3 shows the HSV distribution for the state-space approximation of the surge-surge wave-radiation-retardation kernel, $K_{11}(t)$. Only a small set of states accounts for most of the impulse energy. For instance, the first two states account for 77.5% of the total impulse energy. It is then possible to consider a limited subset of states for the convolution approximation without losing accuracy. The model reduction is carried out in MATLAB by means of the function BALMR (balanced model reduction), which is based on truncation and Shur methods and implemented in Robust Control Toolbox [20,24].

3.3. Viscous drag

In severe sea states, the hydrodynamic loads from linear potential flow theory may be augmented by a term accounting for flow separation [13]. The Morison's formulation, commonly used for the hydrodynamic loads' definition in the analysis of fixed-bottom structures for offshore wind turbines, may be used to define viscous drag loads for cylindrical structures if 1) diffraction effects are negligible in severe sea states, 2) radiation damping is small, and 3) flow separation will occur in severe sea states [5]. Spar structures generally fulfil these requirements. The fluid velocity in surge and sway directions (1 for the surge direction, 2 for the sway direction) is defined from linear potential flow theory as [5,15]:

$$v_1(t,x,y,z) = \frac{cos\psi}{2\pi}\int_{-\infty}^{+\infty} W(\omega)\sqrt{2\pi S^{2-Sided}(\omega)}\, e^{-jk(\omega)[x\cos\psi + y\sin\psi]}\frac{cosh[k(\omega)(z+h)]}{sinh[k(\omega)h]}e^{j\omega t}d\omega \tag{12}$$

$$v_2(t,x,y,z) = \frac{sin\psi}{2\pi}\int_{-\infty}^{+\infty} W(\omega)\sqrt{2\pi S^{2-Sided}(\omega)}\, e^{-jk(\omega)[x\cos\psi + y\sin\psi]}\frac{cosh[k(\omega)(z+h)]}{sinh[k(\omega)h]}e^{j\omega t}d\omega \tag{13}$$

where h is the water depth and $k(\omega)$ is the wave number, defined through the following implicit equation [15]:

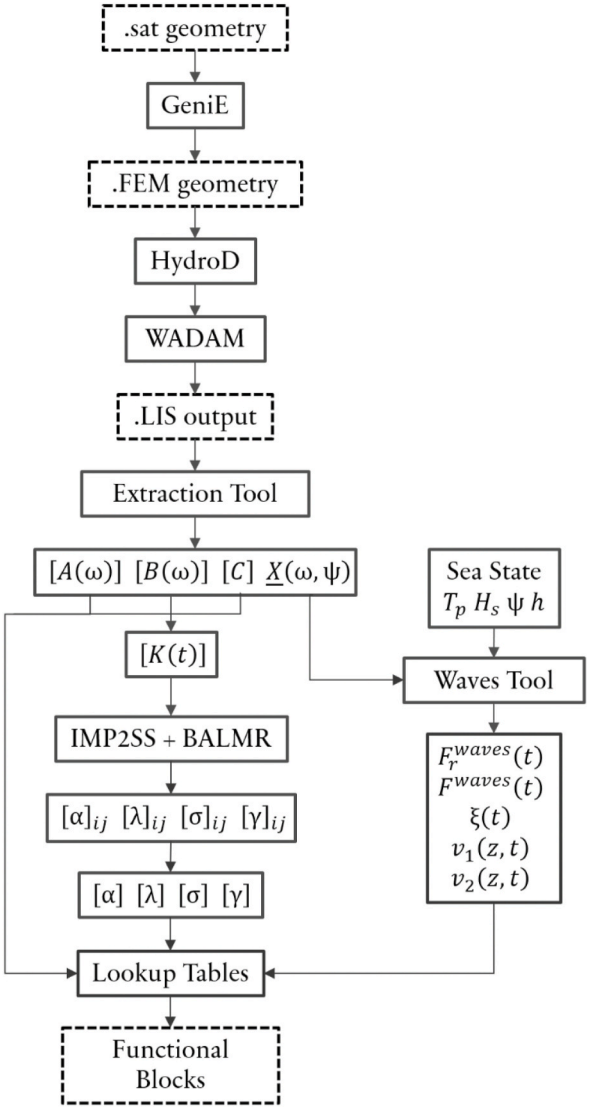

Fig. 4. Hydrodynamic preprocessing workflow (see Section 3.4).

$$k(\omega)tanh[k(\omega)h] = \frac{\omega^2}{g} \tag{14}$$

The viscous drag load can be then defined as:

$$dF_i^{drag}(t,z) = \frac{1}{2}C_d\rho_{water}Ddz\left[v_i(t,0,0,z) - \dot{q}_i(z)\right]|\underline{v}(t,0,0,z) - \underline{\dot{q}}(z)| \tag{15}$$

where C_d is the drag coefficient, D is the spar diameter, dz is the vertical spar section height, and $i = 1$ or 2.

3.4. Preprocessing

In order to define the linear hydrodynamics of a floating body, it is first necessary to solve the frequency-domain hydrodynamic problem by means of numerical-panel codes. The hydrodynamic quantities needed are the added mass matrix $[A(\omega)]$, linear damping matrix $[B(\omega)]$, hydrostatic matrix $[C]$, and the vector of wave loads per unit wave amplitude, $\underline{X}(\omega, \psi)$. In this work, the frequency-domain hydrodynamic problem is solved by means of the industry-standard numerical-panel code WADAM, available within the DNV-GL software SESAM [25].

Fig. 4 shows the preprocessing workflow. First, the wetted surface geometry, generally of arbitrary shape, is provided to the SESAM built-in CAD software GeniE. The extension *.sat* is compatible with the package and can be exported by most commercial CAD software.

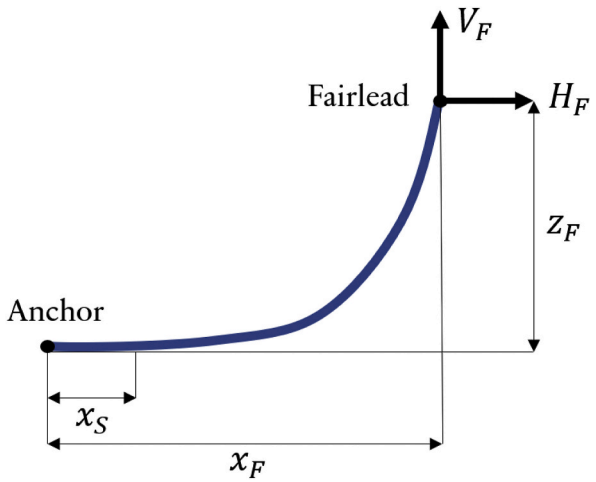

Fig. 5. Mooring line schematization.

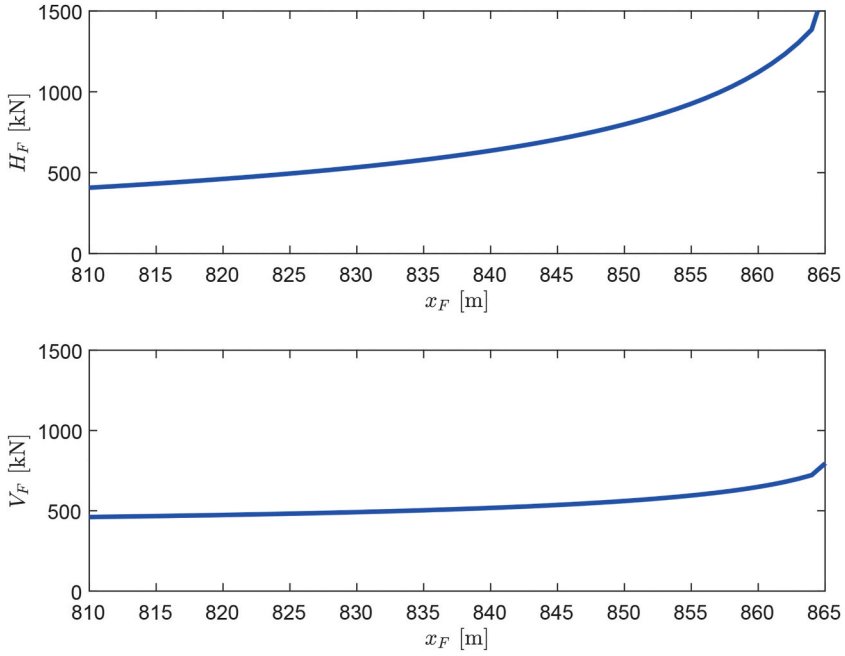

Fig. 6. Mooring line load characteristic (unstretched length 902.2 m, mass density 77.71 kg/m, vertical length 250 m, diameter 0.09 m).

The geometry may also be developed directly in GeniE. Next, the frequency-domain hydrodynamic analysis is carried out in HydroD–WADAM. All the hydrodynamic quantities are computed at the SWL. The resulting output file, with extension *.LIS*, is then processed through an extraction tool developed for the purpose. The tool gives the hydrodynamic quantities in the canonical form. The wave-radiation-retardation kernel matrix is obtained from the frequency-domain damping matrix, $[B(\omega)]$. The state-space approximation of each kernel matrix component *ij* is carried out through employment of the functions IMP2SS and BALMR offered within MATLAB. The single state-space matrices are then assembled, giving rise to the final state-space formulation, $[\alpha]$, $[\lambda]$, $[\theta]$, and $[\gamma]$. Next, a tool for the generation of wave quantities is developed. Inputs of the tool are parameters describing the sea state (T_p, H_s, ψ, h) and the vector of wave-excitation loads on the platform per unit wave amplitude, $\underline{X}(\omega,\psi)$. Outputs of the tool are the time realizations of wave quantities (incident wave loads, wave amplitude, and horizontal fluid velocities). All the quantities thus defined are finally stored in lookup tables communicating with the functional blocks in Modelica.

4. Mooring lines

The implementation includes the nonlinear, quasi-static formulation for the load-displacement relationship of taut or slack

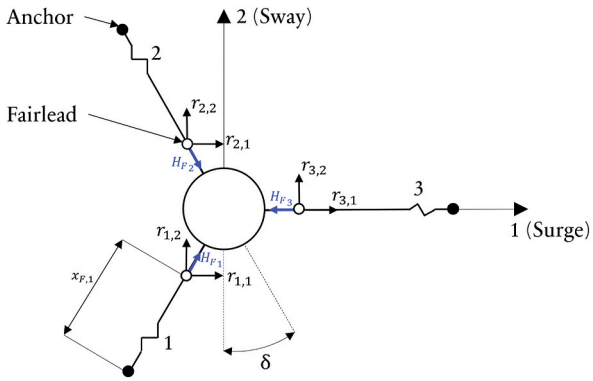

Fig. 7. OC3-Hywind mooring lines schematization (top-view).

catenary mooring lines [5]. Verification and benchmark of the method can be found in Ref. [6]. In this formulation, the fairlead position is known from the global system dynamics, while the mooring tension is computed at each instant by assuming the line in static equilibrium. The quasi-static formulation ignores any mooring line inertia and damping contribution to the system dynamics.

Fig. 5 shows a schematization of a single mooring line. The implicit nonlinear formulation computes the horizontal and vertical loads at the fairlead point, H_F and V_F, as a function of the mooring stretching. Linear yaw stiffness is added to take into account the rigidity given by the mooring lines and bridles [6]. The formulation assumes a portion of the mooring line near the anchor point laying on the seabed, x_S. The mooring stretching is described by means of the fairlead horizontal and vertical distance from the anchor point, x_F, and z_F.

Fig. 6 shows the mooring line load characteristic as a function of the fairlead horizontal and vertical distance from the anchor point. The relationship is strongly nonlinear. Both horizontal and vertical mooring loads experience a steep rise when the mooring line gets more taut - the nonlinear increment is particularly visible for horizontal distances higher than 90% the unstretched mooring line length. Assuming a fairlead vertical distance from the anchor point of about 250 m, the mooring line will be completely detached from the seabed ($x_S = 0$ m) if the horizontal fairlead distance from the anchor point exceeds 858.5 m.

4.1. OC3-hywind mooring lines

Fig. 7 shows a top-view schematization of the standard mooring system employed in the OC3-Hywind spar-buoy platform. The angle δ is equal to 30°. Three independent mooring lines are considered, installed at 120° from one another. The unstretched mooring line length is about 902.2 m. The static mooring line horizontal length, l_0, is about 848.67 m, while the static mooring line vertical length, v_0, is about 250 m [13]. The horizontal and vertical fairleads distance from the anchor points need to be defined in order to determine the mooring loads acting on the platform. To this end, the fairleads displacements in surge and sway direction, computed from the global system dynamics (r_{ij}, where i is the ith mooring line and j is the jth direction) can be projected in the mooring lines local directions. The effective horizontal distances of the fairleads from the associated anchor points can be written as:

$$x_{F,i} = l_0 + \Delta_1(i) r_{i1} + \Delta_2(i) r_{i2} \tag{16}$$

where:

$$\Delta_1(i) = \begin{cases} sin\delta, & \text{if } i = 1 \\ sin\delta, & \text{if } i = 2 \\ -1, & \text{if } i = 3 \end{cases} \tag{17}$$

and:

$$\Delta_2(i) = \begin{cases} cos\delta, & \text{if } i = 1 \\ -cos\delta, & \text{if } i = 2 \\ 0, & \text{if } i = 3 \end{cases} \tag{18}$$

The effective vertical distances of the fairleads from the associated anchor points are determined through the vertical fairleads displacements:

$$z_{F,i} = v_0 + r_{i3} \tag{19}$$

The mooring line horizontal loads, referred to the mooring line local reference frames, need to be referred to the fairlead global reference frame before application. The transformation can be expressed as:

$$\begin{cases} H_{Fi,1} = \Delta_1(i) H_{Fi} \\ H_{Fi,2} = \Delta_2(i) H_{Fi} \end{cases} \tag{20}$$

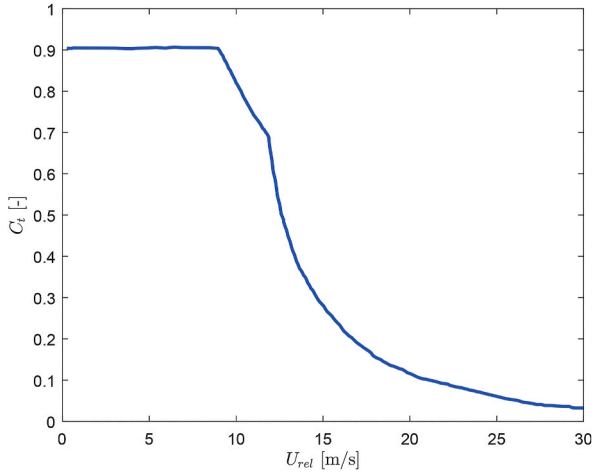

Fig. 8. Thrust coefficient as function of relative wind velocity used in simplified aerodynamic codes [28].

where $H_{Fi,1}$ is the i-th mooring line horizontal load projected in the surge direction. Vertical mooring line loads do not need any transformation.

5. Aerodynamics

5.1. Simplified aerodynamics

Most numerical codes utilized to design FOWTs, such as FAST, HAWC2, and SIMA, incorporate a quasi-static blade element/momentum theory to model blade aerodynamics. The aerodynamic loads acting on the structure are instantaneously computed from the integration of finite-element based drag and lift forces, allowing for very good response precision [26]. Simplified models are also used to define aerodynamic loads, suitable for feasibility and conceptual studies when the effects of rotor dynamics are negligible. Karimirad et al. [27] investigated the response of a dynamic link library called TDHMill (Thrust-Dynamic-Horizontal-Mill), where the aerodynamic loads are defined as an overall concentrated thrust load acting on the hub. The response was compared with the HAWC2 BEM-based code, showing good agreement for operational conditions. Nielsen et al. [28] analyzed the response of an integrated code of FOWTs using a similarly simplified aerodynamics. They compared the code response against an equivalent model scale response, showing good overall agreement. Rotor dynamics, distributed aerodynamic loads, and detailed control dynamics are neglected. This type of simplified aerodynamics computes the thrust force acting on the hub as:

$$F = \frac{1}{2}\rho_{air} C_t(U_{rel}) A U_{rel}^2 \tag{21}$$

where ρ_{air} is the air density, C_t is the thrust coefficient, A is the total aera swept by the rotor, and U_{rel} is the relative velocity between the incoming wind flow and hub:

$$U_{rel} = U_{wind} - U_{hub} \tag{22}$$

U_{wind} and U_{hub} are local projections, transversal to the rotor plane, of the wind and hub velocities referred to the global reference frame. U_{wind} incorporates the 3-dimensional turbulent wind field at the hub.

Fig. 8 shows the thrust coefficient-relative wind velocity relationship used in simplified aerodynamic codes. The thrust coefficient profile incorporates the effect of rotor-collective blade-pitch angle PI control. A notch filter on the tower velocity signal is also incorporated to consider resonant motions above the rated wind speed.

5.2. Steady-state aerodynamics

In the present study, steady-state rotor aerodynamics including a simplified rigid-rotor EoM and a PI rotor-collective blade-pitch controller is implemented. A single-DOF rigid rotor EoM is included in the aerodynamic module. The rotor equation of motion is [5]:

$$\left(I_{rotor} + \gamma^2 I_{generator}\right)\dot{\omega}_{rotor} = T - \gamma T_{generator} \tag{23}$$

where I_{rotor} is the rotor inertia, $I_{generator}$ is the generator inertia, γ is the gearbox ratio, ω_{rotor} is the low-speed shaft rotational speed, T is the aerodynamic torque acting on the low-speed shaft, and $T_{generator}$ is the generator torque acting on the high-speed shaft.

Table 5 shows the main drivetrain properties. $T_{generator}$ is a characteristic of the wind turbine, incorporating variable-speed torque control and given as a tabulated function of the generator rotational speed [5].

Table 5
Drivetrain properties NREL Baseline 5 MW Wind Turbine [5].

I_{rotor}	kgm^2	$3.86x10^7$
$I_{generator}$	kgm^2	534.116
Γ		97
$\omega_{generator,rated}$	rpm	1173.7

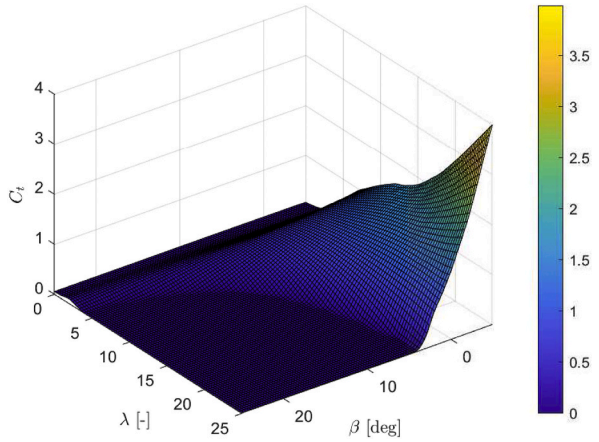

Fig. 9. Thrust coefficient (NREL 5 MW Baseline Onshore Wind Turbine).

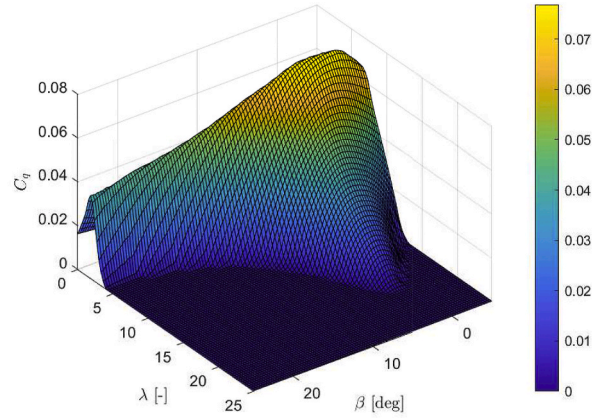

Fig. 10. Torque coefficient (NREL 5 MW Baseline Onshore Wind Turbine).

The aerodynamic loads acting on the system are composed of a concentrated thrust load at the hub and a torque acting on the rotor low-speed shaft. The aerodynamic loads are defined by means of steady-state aerodynamic coefficients. The aerodynamic loads can be written as:

$$F = \frac{1}{2}\rho_{air} C_t(\lambda, \beta) A U_{rel}^2 \tag{24}$$

and:

$$T = \frac{1}{2}\rho_{air} R C_q(\lambda, \beta) A U_{rel}^2 \tag{25}$$

where β is the rotor-collective blade-pitch angle, R is the rotor radius, and λ is the tip speed ratio, defined as:

$$\lambda = \frac{\omega_{rotor} R}{U_{rel,filtered}} \tag{26}$$

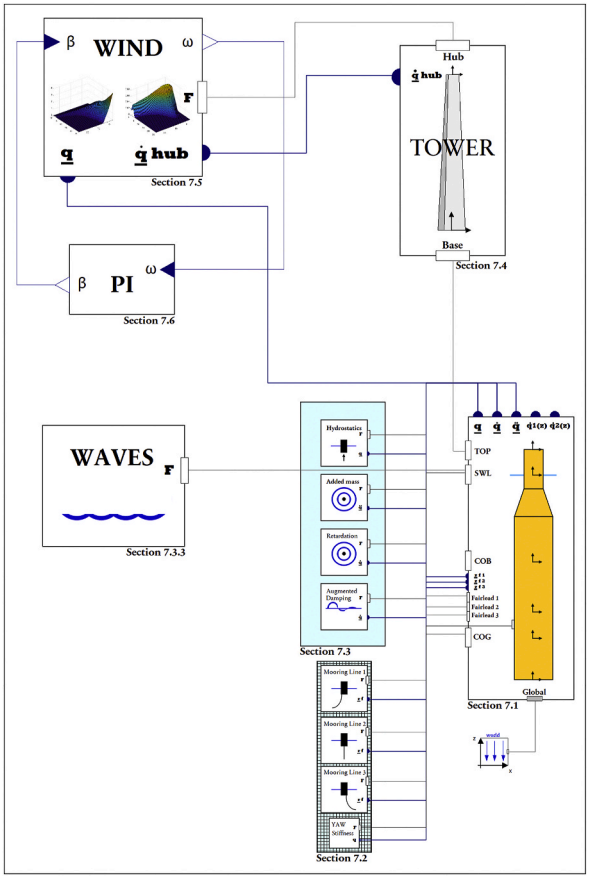

Fig. 11. Diagram view of the OC3-Hywind model implemented in OpenModelica. Blocks are labelled with the associated section of the paper describing their implementation. All the major functional blocks and their interactions are depicted.

where $U_{rel,filtered}$ is the low-pass filtered relative velocity between incoming wind and hub:

$$U_{rel,filtered} = U_{wind,filtered} - U_{hub} \tag{27}$$

The effective decoupling of the rotor-collective blade-pitch angle from the aerodynamics makes this method also suitable for the analysis of blade-pitch control strategies - not possible with simplified tools such as TDHMill. The aerodynamic coefficients are steady-state quantities. In order to avoid unrealistic turbulent coefficients fluctuations, the wind velocity used to define λ only accounts for relatively steady velocity variations by filtering out high frequency content. The wind velocity profiles are obtained through the code NREL-TurbSim. The turbulence model used in this work is the standard Kaimal. An IEC Class B normal turbulence model (NTM) is used. The steady-state aerodynamic coefficients are obtained through the code NREL-FAST for the onshore NREL 5 MW baseline wind turbine. AeroDyn v15 is used to solve the aerodynamics loads. A steady wind profile is used (WindType = 1). A time step of 0.001 s is used. The rotor is assumed to be rigid (CompElast = 1). A steady blade airfoil aerodynamic model is used (AFAeroMod = 1). Blade-pitch control is deactivated. A batch analysis is carried out in order to collect the aerodynamic coefficients profiles. λ is varied between 0 and 25, and β between -5° and 25°.

Figs. 9 and 10 show the obtained thrust and torque coefficients, respectively.

At any rate, the modeling of aerodynamic loads by means of steady-state coefficients naturally leads to unavoidable limitations. Aerodynamic effects induced by unsteady dynamic motions are neglected, such as the effects given by the dynamic inflow, the rotor yaw motion, and the airfoil spatial orientation of the blades. This method is generally suitable to assess only the overall dynamic response of FOWTs, and leads to accurate results only when considering operational environmental conditions [27].

6. Rotor-collective blade-pitch controller

In this work, β is computed by means of a complete PI control of the error between the generator rotational speed and its rated speed value. The control system developed is based on the baseline NREL 5 MW wind turbine PI controller [5]. At below-rated wind speeds, only the variable-speed generator-torque controller is active in order to maximize power output. At above-rated wind speeds, the PI controller is active in order to limit the generator speed to rated values. If the generator rotational speed error is:

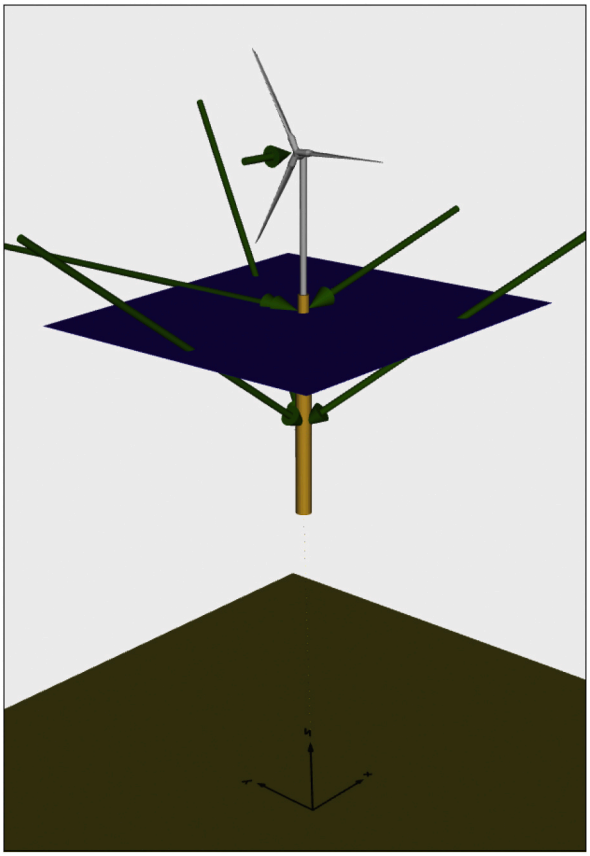

Fig. 12. 3-dimensional representation of the OC3-Hywind model implemented in OpenModelica. Only the thrust load at the hub, the incident wave loads at the SWL, and the mooring loads at the fairleads are depicted (18 m/s, H_s 6 m, T_p 10 s - Aspect Ratio 8e3 N/m, 30e3 Nm/m).

$$f = \left(\omega_{generator} - \omega_{generator,rated}\right) \tag{28}$$

The rotor-collective blade-pitch angle can be computed as:

$$\beta = K_p(\beta) f + K_I(\beta) \int_0^t f dt \tag{29}$$

where $K_p(\beta)$ and $K_I(\beta)$ are the proportional and integral gain-scheduling, respectively. The gains vary to account for a reduction of aerodynamic power sensitivity to rotor-collective blade-pitch angles [5].

7. Modelica implementation

Modelica codes are developed as packages composed of hierarchically-ordered classes. Classes are in this work called functional blocks. Functional blocks are characterized by input/output connectors that allow the exchange of functional quantities. Each functional block is semi-independent, meaning that it only needs the definition of the necessary input quantities in order to be operative. This property is a direct consequence of the object-oriented nature of Modelica and allows for high modeling and debugging flexibility. Specific models are constructed by the deployment of functional blocks. The implementation is carried out in OpenModelica, the major open-source Modelica-based platform. The integration method used is the standard *dassl*, with a tolerance equal to $1x10^{-6}$ and time step equal to 0.1 s. The time step is associated with a Nyquist-bounded maximum dynamic frequency of 5 Hz, well higher than the system natural frequencies and therefore suitable to cover the rigid body dynamics. Fig. 11 shows the diagram view of the OC3-Hywind model implemented in OpenModelica. Each block is labelled with the associated section of the paper describing its implementation. All the major functional blocks and their interactions are depicted. Fig. 12 shows a 3-dimensional representation of the model presented. In the following sections, a general account of the implementation strategy employed is set forth.

7.1. MultiBody implementation

The MultiBody System (MBS) functional block is developed by employing standard MultiBody Modelica Library components. A

bodyShape is used to define the platform equations of motion. The mass matrix is imported from a *.mat* file through the *readRealMatrix* function. Reference frames are defined by means of *FixedTranslations* from the body *frame.a*. Five frames are defined. Three are defined at the corresponding fairlead locations - where dynamic loads associated with the mooring lines are applied. One is defined at the COG location - where hydrostatic restoring loads are applied. Finally, one is defined at the SWL location - where the linear hydrodynamic loads are applied. The body is referred to the global reference frame, placed at the seabed location, by means of a *freeMotion* joint. The initialization of the MBS state is enforced at the *freeMotion* level. A *fixedShape* is used to import ASCII encoded.stl CAD geometry of the system for animation. The body displacements, velocities, and accelerations computed at the SWL ($\underline{q}$, $\underline{\dot{q}}$, and $\underline{\ddot{q}}$) are exchanged with other functional blocks by means of *RealVectorOutput* connectors. The fairleads displacements ($\underline{r_{ij}}$) are exchanged in the same manner with the mooring lines functional blocks. The body velocity in surge and sway directions as function of water depth ($\underline{\dot{q}_1}(z)$ and $\underline{\dot{q}_2}(z)$) are computed through a two-point linear interpolation and exchanged with the viscous drag functional block.

7.2. Mooring lines implementation

Specific functional blocks are implemented for each mooring line. Table look-up in two dimensions is carried out by means of the *combiTable2D* block, in order to compute the mooring loads given the effective fairleads distances from the associated anchor points. The fairleads displacements are exchanged from the MBS functional block as input to the mooring functional blocks. The mooring loads at the fairleads are exchanged from the mooring functional blocks as input to the MBS functional blocks and applied at the fairlead frames. Vertical mooring dynamics is implemented as an optional feature. In the case the vertical mooring dynamics is operative (default), an additional vertical static load equal to the vertical static preload of the mooring line is activated. The static preload of the mooring line is automatically computed by means of an additional table look-up for the vertical mooring load, whose input is the fairlead position computed at $t = 0$ s. The computation of the unstretched mooring line length resting on the seabed is also implemented. All the loads are defined as *WorldForce* and resolved in the world frame. The mooring loads are applied to the system at time 0.1 s, in order to aid the integrator initialization process. An additional yaw spring stiffness of about $9.8x10^7$ Nm/rad is also applied [13].

7.3. Linear hydrodynamics implementation

7.3.1. Linear relationships

In order to implement linear relationships, such as the hydrostatic restoring loads, the added mass loads, and the additional damping loads, the associated *.mat* matrices are imported through the *readRealMatrix* function. Input state vectors ($\underline{q}$, $\underline{\dot{q}}$, or $\underline{\ddot{q}}$) are exchanged from the MBS functional block. The related linear loads are obtained by scaling the input state vector with the associated matrix. Loads are defined as WorldForce and resolved in the world frame. All linear hydrodynamic load contributions need to be applied at the location where the preliminary frequency-domain hydrodynamic problem is solved - in this case at SWL. Hydrostatic relationships are instead applied at COG since hydrostatic restoring torques are also defined through metacentric height relationships. The total buoyancy force from Archimedes' principle is implemented through a static *WorldForce* directed upwards and resolved in the world frame.

7.3.2. Wave-radiation damping

The wave-radiation damping functional block is implemented by means of the standard block *StateSpace*, solving a state-space system given the input vector. State-space variables are forced to initialize at zero. The input vector is set equal to the velocity state vector exchanged from the MBS functional block, $\underline{\dot{q}}$. The assembled *.mat* state-space matrices are imported through the standard *readRealMatrix* function. All the loads are defined as WorldForce and resolved in the world frame.

7.3.3. Incident wave loads

Incident wave loads time realizations are implemented through the standard *CombiTimeTable* block, which allows for table look-up with respect to time and linear-periodic interpolation. Look-up start time is set to 0.1 s, in order to aid the integrator initialization process. A continuous-derivative smoothness of table interpolation is used.

7.3.4. Viscous drag

Time realizations of surge and sway water velocity fields, varying with water depth, are also implemented through the standard *CombiTimeTable* block. Look-up start time is set to 0.1 s. Body velocity in surge and sway directions as function of water depth ($\underline{\dot{q}_1}(z)$ and $\underline{\dot{q}_2}(z)$), defined through two-point interpolation, are exchanged from the MBS functional block to the viscous drag functional block. Morison's definition of drag loads included the platform diameter variation. The platform discretization step, dz, is set equal to 1 m.

7.4. Tower

The tower functional block is needed to define a reference frame local to the hub. In order to do so, *fixedTranslations* are used. The hub velocity vector, $\underline{\dot{q}_{hub}}$, is also exchanged from the tower functional block to the aerodynamic module.

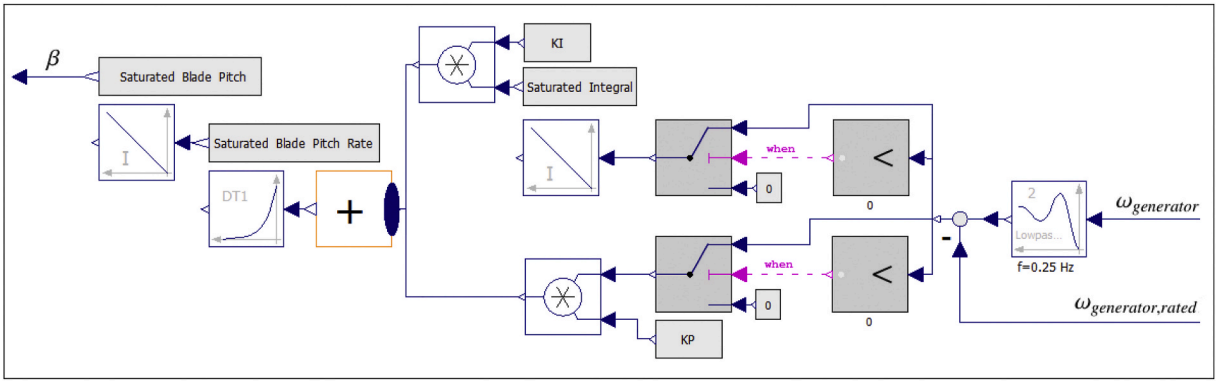

Fig. 13. Block Diagram of the Baseline Rotor-Collective Blade-Pitch PI controller implemented in OpenModelica.

Table 6
Summary of the modeling capabilities of the major codes used in the code-to-code comparative analysis [4,29,30]. (T: Turbine. P: Platform. Mod: Modal dynamics. MBS: Multi-Body System. FE: Finite-Element. SS: Steady-State. QS: Quasi-Static. BEM: Blade Element/Momentum. PF: Potential Flow. ME: Morison's Equation.)

Code	Developer	Structural Dynamics	Aerodynamics	Hydrodynamics	Mooring Dynamics
Present Model	–	T: Simplified P: Rigid	SS	PF + ME	QS
FAST	NREL	T: Mod/MBS P: Rigid	BEM	PF + ME	QS
Simo-Riflex	MARINTEK	T: FE P: FE	BEM	PF + ME	FE
HAWC2	DTU Wind	T: MBS/FE P: MBS/FE	BEM	ME	FE
GH Bladed	DNV GL	T: Mod/MBS P: Rigid	BEM	PF + ME	QS

Table 7
Load cases (LCs) used in code-to-code comparative analysis, based on IEA Phase IV [29].

LC	Wind Conditions	Wave Conditions	Type
1.2	None: air density = 0	Still Water	Eigenanalysis
1.4	None: air density = 0	Still Water	Free-decay test time series
4.1	None: air density = 0	Regular Airy: $H_s = 6$ m, $T_p = 10$ s	Periodic time series
4.1*	None: air density = 0	Regular Airy: $H_s = 2$ m, $T_p = variable$	RAOs
4.2	None: air density = 0	Irregular Airy: $H_s = 6$ m, $T_p = 10$ s, JONSWAP spectrum	Power spectra
5.1	Steady, uniform, no shear: $V_{hub} = 8$ m/s	Regular Airy: $H_s = 6$ m, $T_p = 10$ s	Periodic time series
5.3	Turbulent: $V_{hub} = 18$ m/s, I = 0.18	Irregular Airy: $H_s = 6$ m, $T_p = 10$ s, JONSWAP spectrum	Power spectra

7.5. Steady-state aerodynamics implementation

Table look-up in two dimensions is carried out by means of the *combiTable2D* block, in order to compute the aerodynamic thrust and torque coefficients given the tip speed ratio, λ, and the rotor-collective rotor-pitch angle, β. Time realizations of the wind turbulent velocity field, obtained in TurbSim, are implemented through the standard *CombiTimeTable* block. The start time is set to 1 s. The hub velocity vector, $\underline{\dot{q}_{hub}}$, is exchanged from the tower functional block to the aerodynamic functional block. The input state vector, $\underline{q}$, is exchanged from the MBS functional block to the aerodynamic functional block, in order to project the wind and hub velocity transversal to the rotor plane. The filtered turbulent wind velocity needed to compute λ is implemented by means of a *LowpassButterworth* filter with a cut-off frequency set to 0.0033 Hz (5 min cut-off period). Table look-up in one dimension is carried out by means of the *CombiTable1Ds* block, in order to compute the generator torque given the generator rotational speed. β is exchanged from the PI control functional block to the aerodynamic functional block. Conversely, the generator speed, $\omega_{generator}$, is exchanged from the aerodynamic functional block to the PI control functional block. The thrust force is defined as *WorldForce* and resolved in the hub local reference frame. Rotor animation is also implemented by means of a FixedShape attached to a dummy *Revolute* DOF. The rotor position is defined by integration of the rotor rotational speed. A smooth initialization of the aerodynamic module is implemented by adjusting initial values of λ and thrust force. λ is imposed equal to 1 for the first 5 s of the analysis. The thrust force is set equal to 0 N for the first 2 s of the analysis, and equal to $2x10^5$ N for the next 200 s.

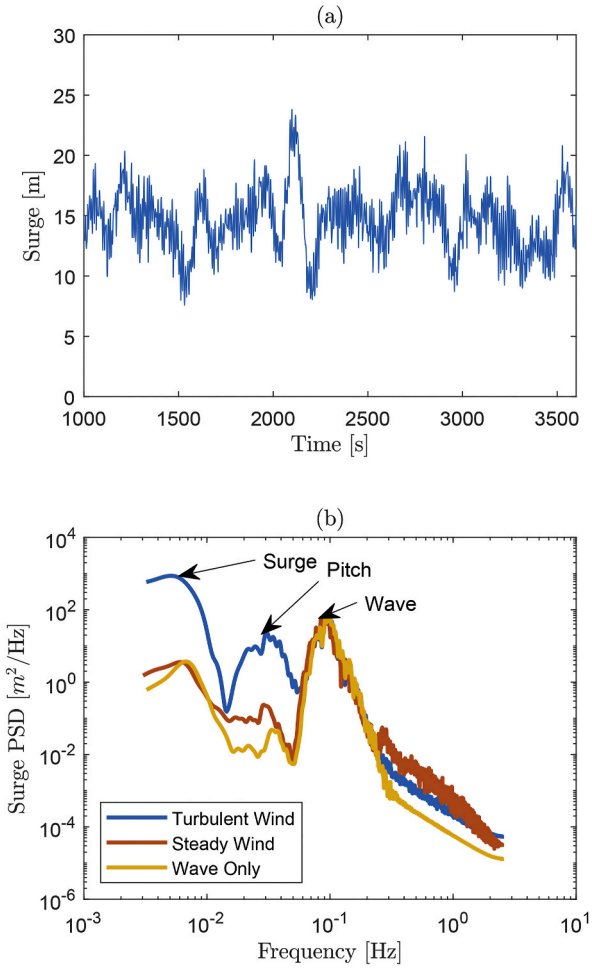

Fig. 14. Surge response for coupled wave-wind analysis. a) Surge time history at SWL for irregular waves and turbulent wind (JONSWAP $H_s = 6$ m and $T_p = 10$ s, V = 18 m/s, I = 0.167). b) Surge smoothed power spectral densities based on 1-h time history in the case of turbulent wind, constant wind, and wave-only conditions.

7.6. Rotor-collective blade-pitch controller implementation

Fig. 13 shows the block diagram of the baseline rotor-collective blade-pitch controller implemented in OpenModelica. The generator rotation speed is exchanged from the aerodynamics functional block to the PI controller functional block. Conversely, β is exchanged from the PI controller functional block to the aerodynamics module. A *LowpassButterworth* filter with a cut-off frequency set to 0.25 Hz is applied to the generator speed signal. The feedback signal is given in rad/s. Standard gain-scheduling laws from the NREL baseline 5 MW onshore wind turbine are used [5]. Table look-up in one dimension is carried out by means of the *CombiTable1Ds* block in order to compute the proportional and integral gains given the blade-pitch angle value. Gain reduction factors are applied to account for smaller gain values employed in offshore applications (0.1 integral gain reduction factor, 0.33 proportional gain reduction factor). A *greaterThreshold* Boolean block is used together with a switch Boolean block to activate the PI controller only when the generator rotational speed reaches rated values. The switch selects between zero and the feedback signal. The integral signal is computed by means of the Integrator block. The integral signal is saturated with saturation limits equal to:

$$\begin{cases} I_{max} = \dfrac{\beta_{max}}{K_I} \\ I_{min} = 0 \end{cases} \tag{30}$$

where K_I is the reduced integral gain scheduling-law, and β_{max} is set to 25°. The blade-pitch rate is obtained by deriving the blade-pitch signal by means of the Derivative block. Saturation of the blade-pitch rate is implemented. A maximum absolute blade-pitch rate equal to $8^\circ/s$ is used. The final blade-pitch signal is computed by integrating the blade-pitch rate signal. A saturation of blade-pitch values is imposed on the final blade-pitch signal. Blade-pitch values between 0° and 25° are enforced.

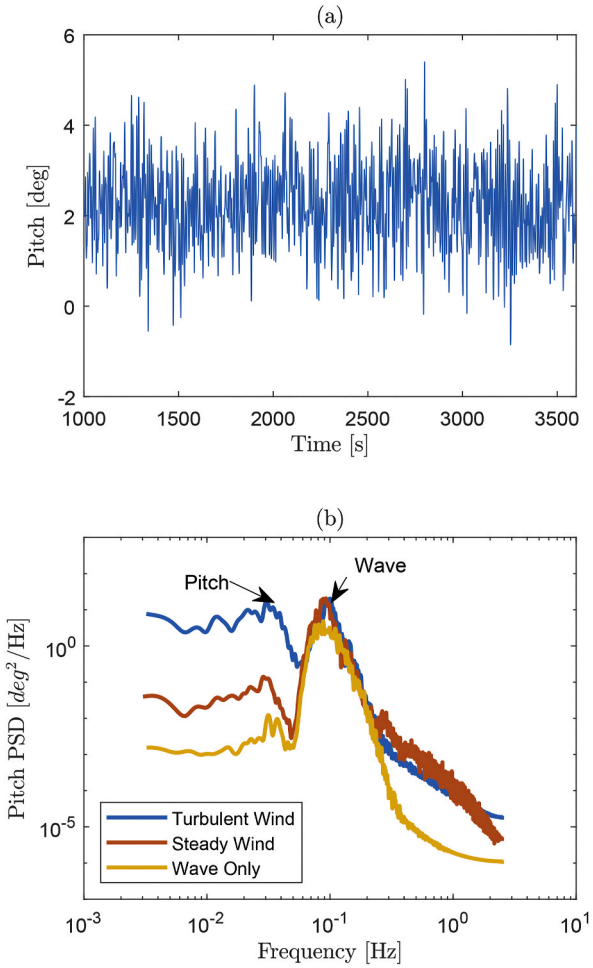

Fig. 15. Pitch response for coupled wave-wind analysis. a) Pitch time history at SWL for irregular waves and turbulent wind (JONSWAP $H_s = 6$ m and $T_p = 10$ s, V = 18 m/s, I = 0.167). b) Pitch smoothed power spectral densities based on 1-h time history in the case of turbulent wind, constant wind, and wave-only conditions.

8. Code-to-code comparative analysis

In this section, a code-to-code comparative analysis is performed by contrasting the dynamic responses of major design codes against the dynamic response of the present model developed in OpenModelica.

Table 6 summarizes the modeling capabilities of the major codes used in the validation analysis. Modeling capabilities are described in terms of methods for structural dynamics, aerodynamics, hydrodynamics, and mooring dynamics modeling. To be noted that most codes use BEM to model blade aerodynamics. The present model is the first to introduce steady-state approach to model blade aerodynamics. The load cases (LCs) used for the analysis are based on the standard International Energy Agency (IEA) Wind Task 23, Phase IV [29,30]. The main reference code used for the comparison analysis is NREL FAST. The comparison is carried out in terms of eigenvalue analysis, free-decay time series tests, and time series and power spectra associated to different load conditions.

Table 7 outlines the LCs used in the comparative analysis. The eigenvalue analysis is performed by linearizing the system in the neighbourhood of its static equilibrium position when neither wind nor wave is acting (system stationary in still water). The initial conditions of the system needed to compute the free-decay response are dynamically initialized by means of a static global force/torque acting in the prescribed DOF. The load is gradually driven from zero to its maximum magnitude, maintained at constant magnitude, and abruptly set to zero when the desired initial conditions are reached. This procedure is implemented by means of a combination of *pulse* and *ramp* blocks as sources for the definition of the load magnitude. A drag coefficient $C_d = 0$ is used. The total simulation time is set to 600 s. The values of H_s and T_p in LC 4.1* are employed in order to compute the RAOs of the system. RAOs are frequency response functions defined as the ratio of a given DOF response amplitude to a given regular wave amplitude. RAOs are used in the offshore oil and gas industry to assess the frequency-domain linear wave-body response of floating platforms. RAOs of spar-buoy platforms are significant only in heave, pitch, and surge direction. OC3-Hywind RAOs computed by means of NREL FAST-HydroDyn are used as main reference [14,31,32]. Regular waves are employed to compute the RAOs (LC 4.1*). For each wave period considered,

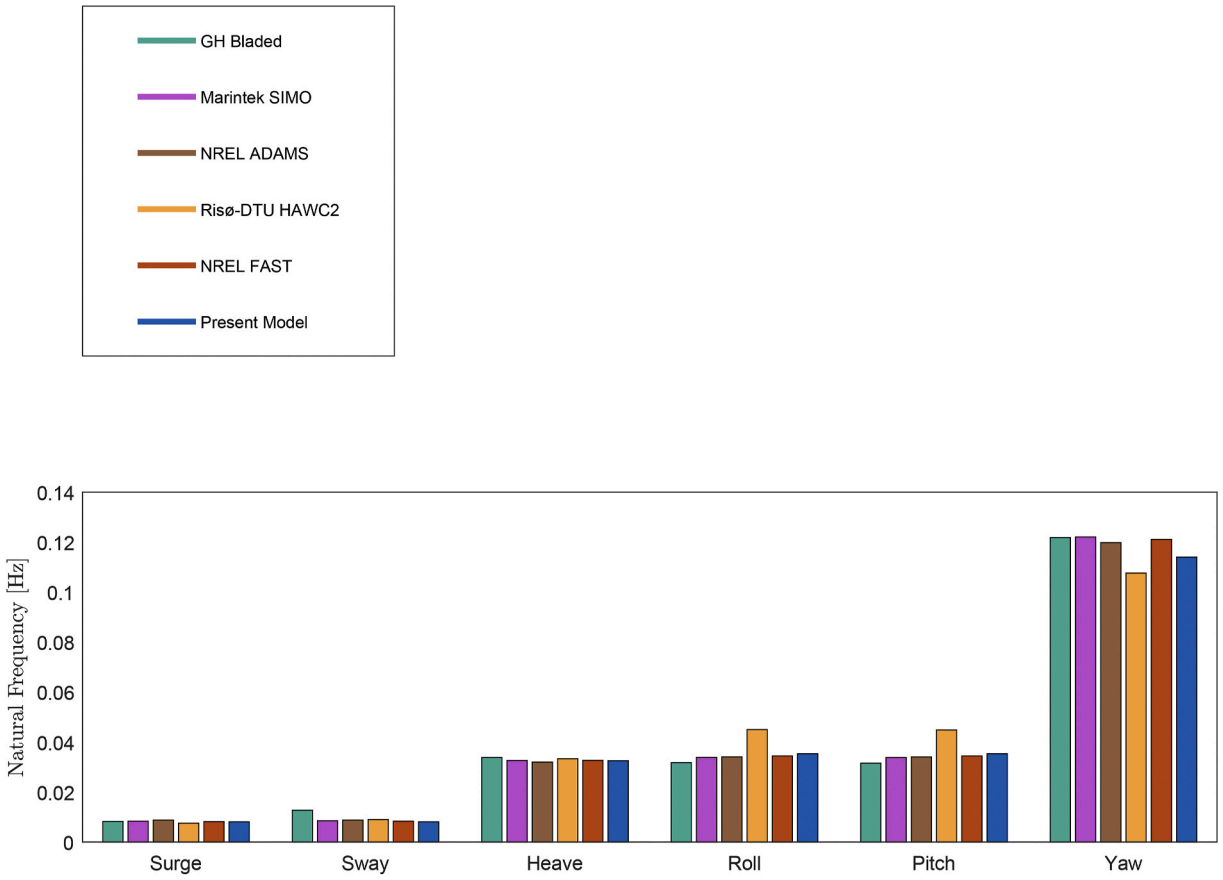

Fig. 16. Full-system hydro-elastic natural frequencies from LC 1.2 [29,30].

the hydrodynamic loads related to a 1 m amplitude regular wave are applied to the system. Because the procedure is based in the time-domain and only a limited number of wave periods is considered, the obtained RAOs are discrete. A drag coefficient $C_d = 0$ is used. The first 600 s are not considered in order to discard initial transients. In order to compute the PSDs of the system response to irregular waves and turbulent wind (LC 4.2 and LC 5.3), a simulation time of 4000 s is carried out. The first 400 s are not considered in order to discard initial transients so that a net 1-h simulation time is used in the analysis. A 15th order one-dimensional median filter is used to smooth the PSD responses.

8.1. *Wind-wave dynamic response*

Figs. 14 and 15 present an example of dynamic response of the system subjected to irregular waves and turbulent wind in terms of surge and pitch response. The dynamic loading of the system is relative to JONSWAP irregular airy waves ($H_s = 6$ m and $T_p = 10$ s), and turbulent wind (V = 18 m/s, I = 0.167). The figures present time series at SWL, and smoothed PSDs based on 1-h time history in the case of turbulent wind, constant wind, and wave-only conditions. Mean displacement values of the system can be inferred from the time histories. PSDs distribution clearly highlights energy peaks at surge, pitch, and wave excitation frequencies.

8.2. *LC 1.2 - full-system eigenanalysis*

Fig. 16 shows the natural frequencies of the rigid motions of the system calculated through eigenvalue extraction. Most of the codes agree in their prediction, except for higher roll/pitch natural frequency computed with HAWC2. Results obtained from present model are in good agreement with most codes, and match very well with the results obtained from the main reference, NREL FAST.

8.3. *LC 1.4 - free decay*

Fig. 17 shows the free decay time series comparison in platform heave, pitch, and surge. The free-decay time series obtained from present model are compared against NREL FAST, and other codes whose free decay responses are available. A certain degree of variability is to be expected among responses obtained through different design codes. For the surge free-decay test, most of the codes

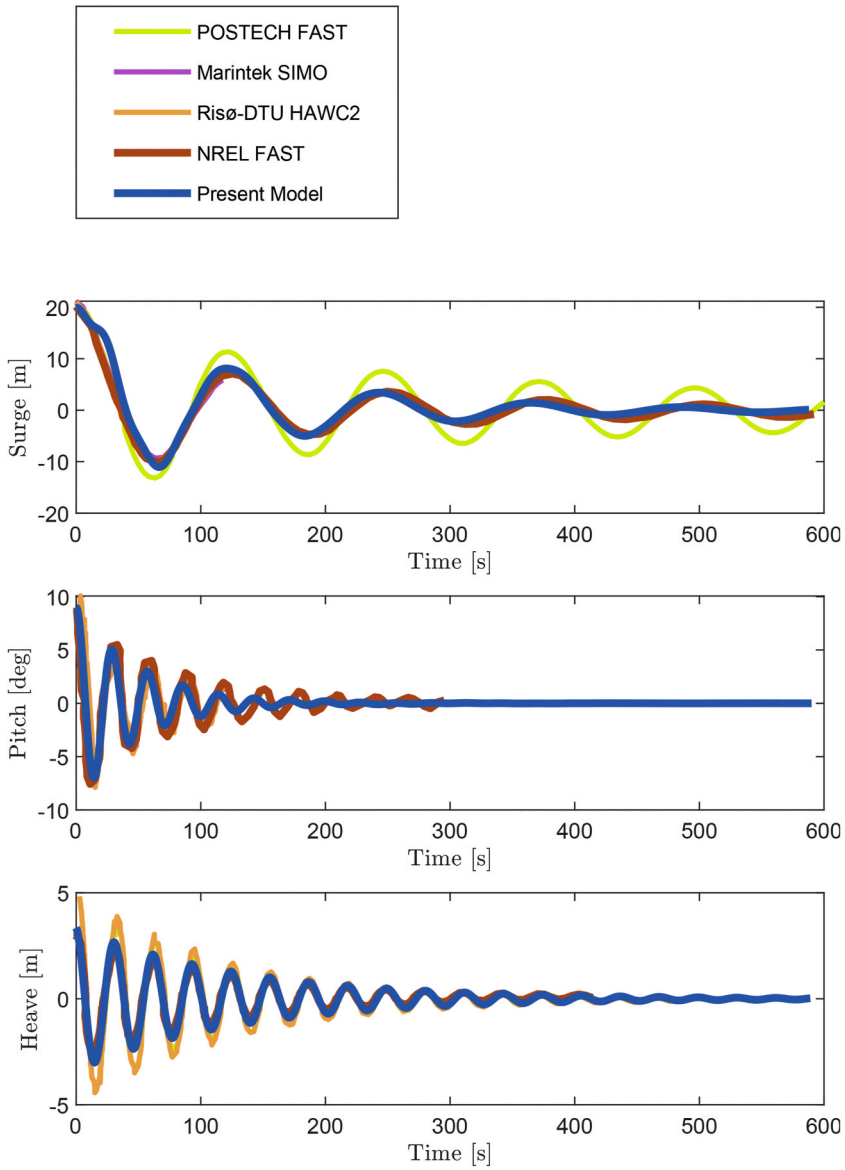

Fig. 17. OC3-Hywind free decay time series comparison in heave, pitch, and surge directions from LC 1.4 [29,30].

Table 8
Natural frequencies of the OC3-Hywind floating wind turbine obtained from present model through free decay tests.

Motion	Natural frequency [Hz]
Surge/Sway	0.0081
Pitch/Roll	0.035
Heave	0.0314
Yaw	0.122

Table 9
Specifications for computing unit used in performance analysis.

CPU	Intel Core i7 9700 3.0 2666 MHz 12M8C 65 W
RAM	64 GB DDR4 2666 DIMM
Drive	512 GB M.2 2280 PCIe NVMe SolidState

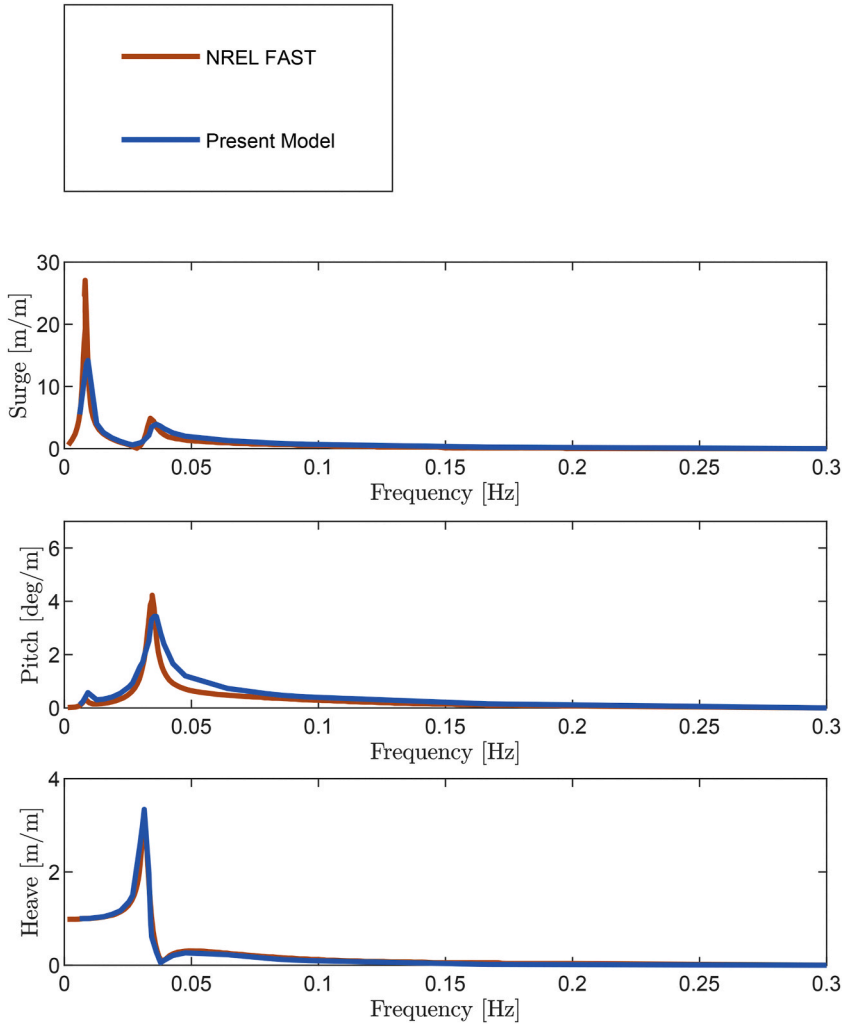

Fig. 18. Response amplitude operators from LC 4.1∗[14].

agree with each other well. POSTECH FAST shows less hydrodynamic surge damping. This discrepancy is due to the lack of additional linear damping in POSTECH results [29]. Results obtained from present model agree very well with FAST results. For the pitch free-decay test, most codes agree. Present model results show a slight difference of pitch natural frequency with respect to results obtained with FAST – about 2.5% higher from present model. The difference is reasonably limited (δ: 9e-4 Hz, min: 0.0316 Hz, max: 0.0448 Hz, σ: 0.0047 Hz). For the heave free-decay test all codes agree, except HAWC2 results which show less hydrodynamic damping. Table 8 shows the natural frequencies of the OC3-Hywind system obtained in present model through free decay tests. The results agree with eigenanalysis.

8.4. LC 4.1∗ - Response Amplitude Operator (RAO)

Fig. 18 shows the RAOs comparison in heave, pitch, and surge motions of the platform. The blue line represents the discrete RAOs obtained from present model. The red line represents the main reference RAOs obtained from FAST-HydroDyn [13,14]. RAOs computed in present model and the ones computed from FAST are in good agreement. The heave RAO approaches unity in the quasi-static region, which is a good quality check for RAOs estimation and agrees well with the reference. Hydrodynamic pitch-surge coupling is clearly visible and is correctly detected both in surge and pitch motions of the platform. A marginally higher amplitude response is experienced in present model in the upper-resonance region, which is most likely associated to the minor shift in the pitch hydrostatic natural frequency between the two codes.

8.5. LC 4.1 - hydro-elastic Response with regular waves

Fig. 19 shows the time series of surge, pitch, and heave motions of the platform, and downstream fairlead tension (mooring line #3 -

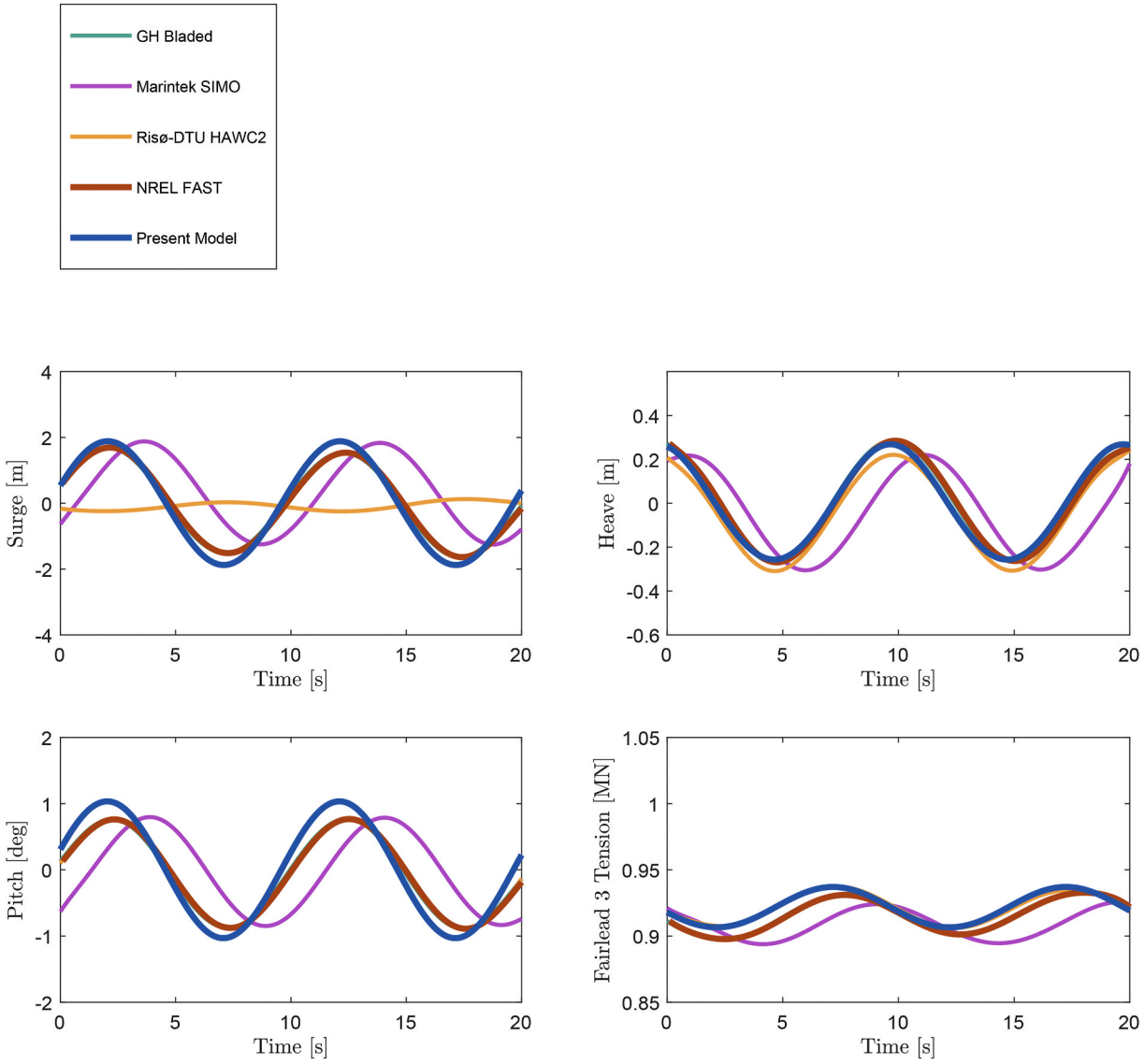

Fig. 19. Hydro-elastic time series with regular waves from LC 4.1 [29,30].

see Fig. 7) under conditions given in LC 4.1. All of the platform initial transients obtained from all codes are removed from the results. All codes agree except HAWC2 surge response, which may simply have output the wrong parameter [29]. SIMO results are phase-shifted relative to the other codes. Present model response agrees very well with NREL FAST response.

8.6. LC 4.2 - hydro-elastic Response with irregular waves

Fig. 20 shows the power spectral densities for the same parameters used in Fig. 19, computed under conditions given in LC 4.2. All codes removed initial transients from the results. A net 1-h simulation time history is used in the PSD computation. Spectral shape estimates obtained from present model agree well with the main reference FAST. Wave energy is mainly distributed at wave excitation frequency, i.e., 0.1 Hz. The distribution of energy at surge, pitch, and wave frequencies obtained with present model agrees well with NREL FAST.

8.7. LC 5.1 - fully-coupled Response with regular waves

Fig. 21 shows the time series of surge, pitch, heave, and yaw motions of the platform, and downstream and upstream fairlead tensions (mooring line #2 and #3 - see Fig. 7) under conditions given in LC 5.1. Nonzero thrust associated with the steady wind causes nonzero mean loads and displacements. SIMO results are phase-shifted relative to the other codes. For the surge displacement, all codes

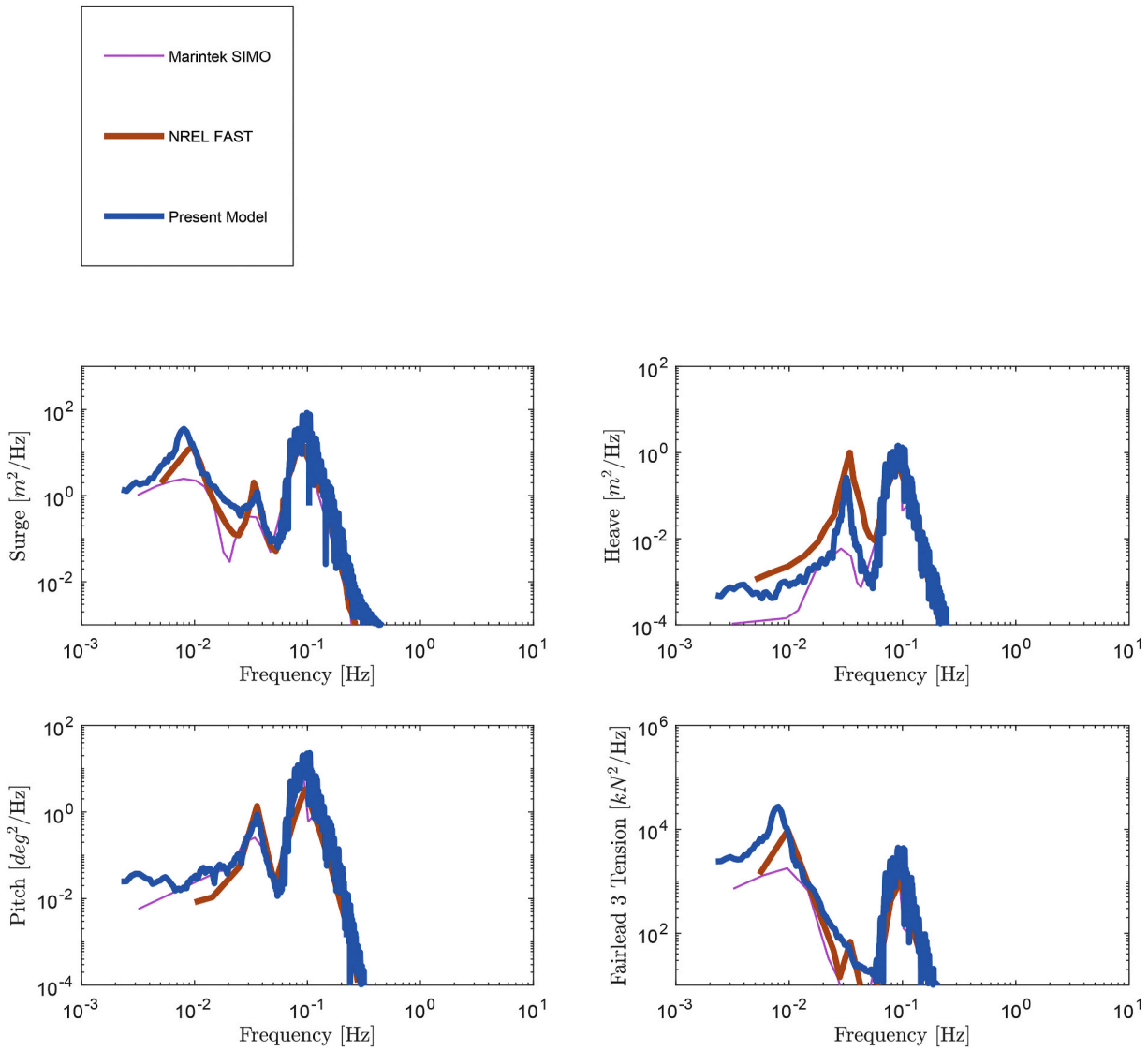

Fig. 20. Hydro-elastic power spectral densities with irregular waves from LC 4.2 [29,30].

except HAWC2 agree well on the oscillation amplitude. The mean surge displacement varies slightly among codes. The mean surge displacements obtained with SIMO and with present model are in a similar fashion slightly higher than the same results obtained from FAST. These differences are, however, reasonably limited ($\delta = 1.5$ m, min: 8.37 m, max: 15.10 m, σ: 2.66 m). The significant difference in yaw response among codes is clearly visible in the figure. Present model yaw response is significantly lower than the response obtained from FAST. The difference is mainly due to the simplified rotor dynamics assumptions employed in the present model. Lack of pitch-yaw coupling given by rotor gyroscopic effects lead to significant difference on yaw dynamics.

8.8. LC 5.3 - fully-coupled Response with irregular waves

Fig. 22 shows the PSDs for the same parameters used in Fig. 21, computed under conditions given in LC 5.3. Initial transients from the results obtained from all codes are removed. A net 1-h simulation time history is used in the PSD computation relative to present model. Spectral shape estimates obtained from present model, given in terms of distribution of energy at surge, pitch, and wave frequencies, agree well with those obtained from FAST. As previously noted in LC 4.2, wave energy is highest at wave excitation frequency, i.e., 0.1 Hz, and most are in good agreement on wave energy distribution. Wind energy is mainly distributed in the low-frequency region – corresponding to the highest energy of the wind [29]. Also in this case, yaw response deviates significantly due to simplified rotor dynamics. The low-frequency yaw response is negligible in present model due to the lack of pitch-yaw coupling induced by the rotor dynamics. The high-frequency yaw response is negligible in present model, also affected by the lack of drivetrain dynamics. Yaw dynamics is then effectively decoupled from the overall wind-induced response in the present model, and the energy

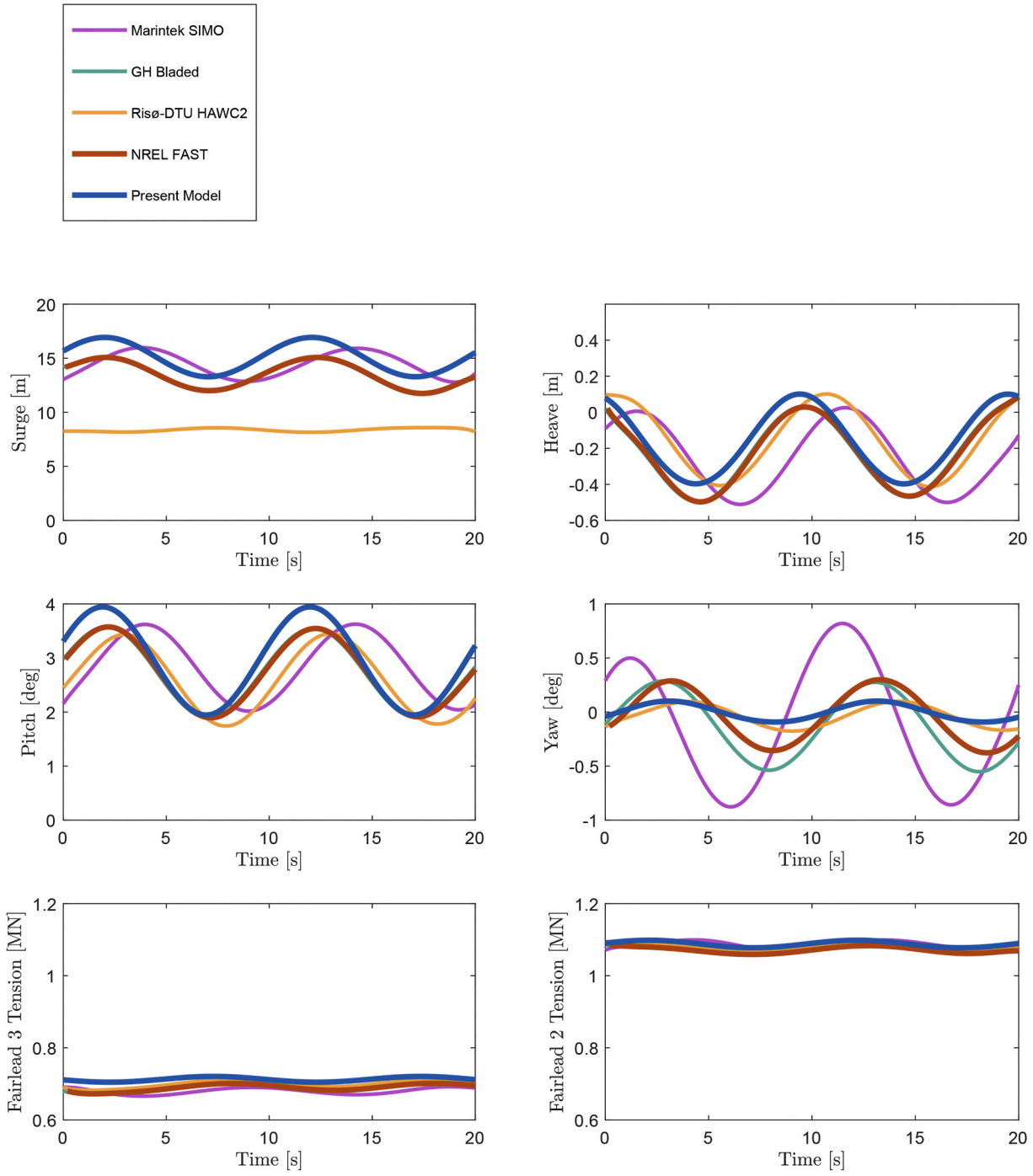

Fig. 21. Fully-coupled time series with regular waves and steady wind from LC 5.1 [29,30].

content in the yaw PSD is mainly associated with the wave loads. Therefore, yaw inaccuracy should be considered as one of the major limitations of this method when considering OC3-Hywind applications.

9. Performance analysis

Performance analysis is conducted in order to quantify the performance of the present model developed in OpenModelica. Simulation time in OpenModelica is compared to the simulation time of NREL FAST. The standard 'CertTest24', modeling OC3-Hywind dynamics, is employed in FAST. The rotor is assumed rigid (BeamDyn deactivated). MAP++ is used to model the mooring system.

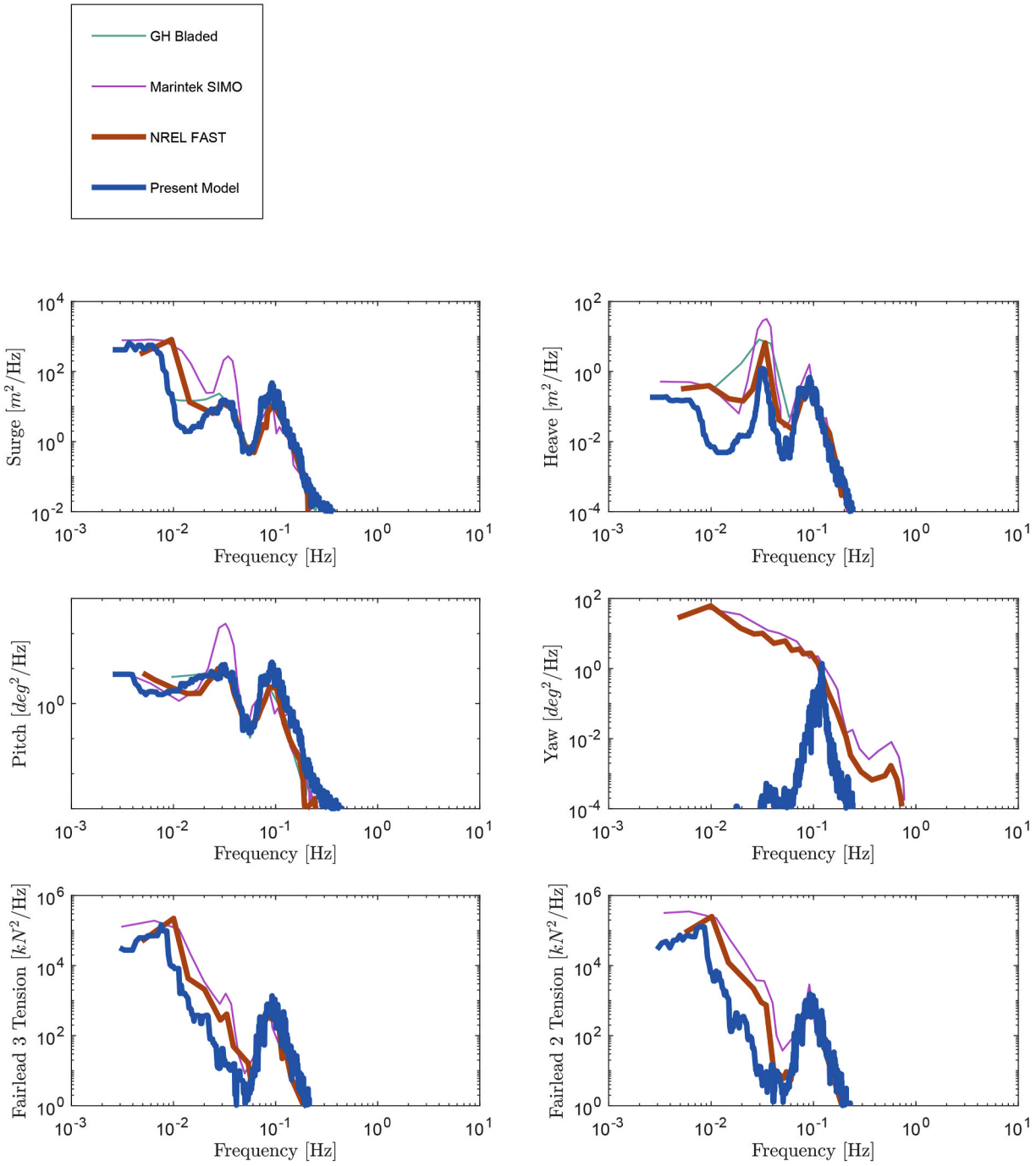

Fig. 22. Fully-coupled power spectral densities with irregular waves from LC 5.3 [29,30].

ServoDyn is used to model drivetrain dynamics. No sub-structural dynamics is considered (SubDyn deactivated). AeroDyn v15 is used to compute aerodynamic loads. InflowWind is finally employed to compute the inflow wind velocity profiles. Environmental conditions considered are based on LC 5.3. Table 9 shows the specifications of the computing unit used to gather performance data. Fig. 23a compares the CPU time relative to the simulated time. Fig. 23b compares the time ratio (defined as the ratio between simulated time and CPU time) relative to the simulated time. As it can be noted from the results, the present model is significantly faster than FAST. For instance, 1-h simulation time needs 19 min ca. in FAST, whilst 2 min are enough to perform the analysis using present model. It can be noted how the time ratio obtained with OpenModelica decreases for shorter simulation times. This may be associated to initial stabilization of *dassl* integration. At any rate, the speed gain with respect to FAST performance is always found to be significant.

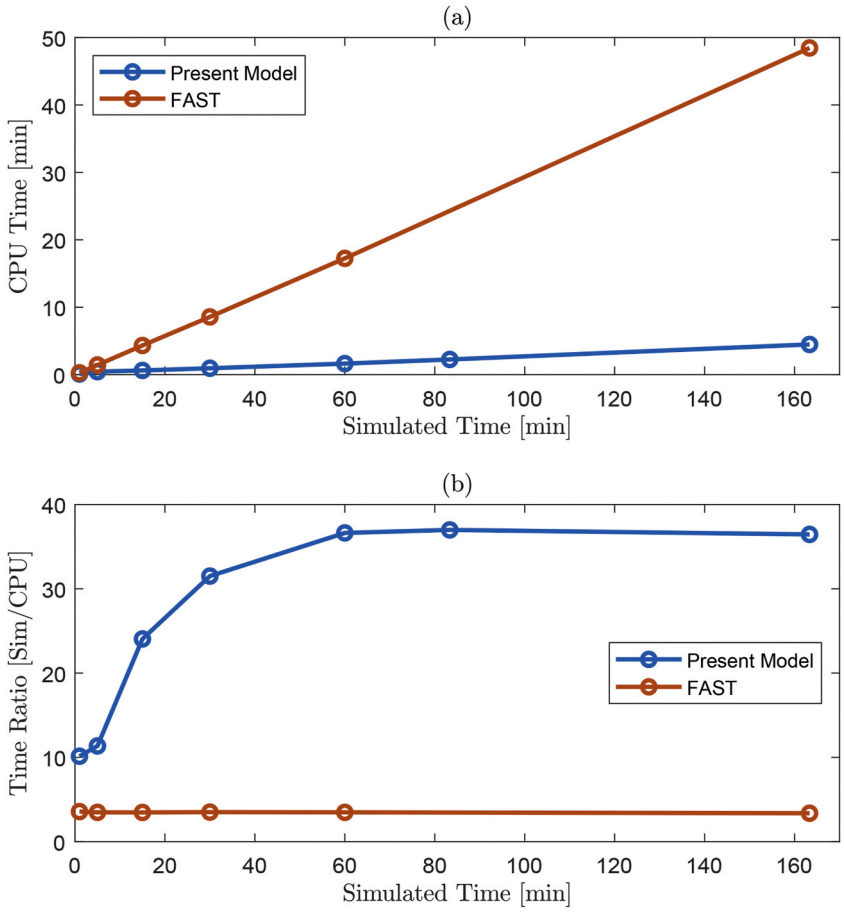

Fig. 23. Comparison of numerical code performance for the present model versus comprehensive code FAST. Standard CertTest 24 is used to compute CPU time (no BeamDyn, MAP++, ServoDyn, no CompSub, AeroDyn v15, InflowWind from TurbSim). Specifications of the computing unit used are listed in Table 9 a) CPU time relative to simulated time. b) Time ratio relative to simulated time.

10. Conclusions

Simplified models covering most of the system dynamics in operational conditions are useful alternatives when working on conceptual studies. The present method is a highly efficient and yet accurate alternative to the commonly-used BEM tools for the fully-coupled dynamic analysis of FOWTs. This method can be very easily adapted to arbitrary platform geometries and platform/rotor configurations. Moreover, the object-oriented structure of the method makes it extremely flexible. The aerodynamic model computes the aerodynamic loads through the mapping of steady-state aerodynamic coefficients. MSL code is employed. The system is assumed as a rigid body. The Airy linear theory is used to implement the hydrodynamic loads given an arbitrary platform geometry. The industry standard numerical-panel code SESAM-WADAM is used to solve the frequency-domain hydrodynamic problem. OC3-Hywind design is used as a reference for the work. A simplified rigid rotor EoM is used to compute the aerodynamic state of the system. A complete PI controller is used to define the rotor-collective blade-pitch angle. The aerodynamic loads are simplified by a concentrated thrust force acting on the hub, and a torque acting on the equivalent rotor low-speed shaft. The mapping of aerodynamic coefficients is carried out in FAST. The turbulent wind velocity relative to the hub motion is used to define the aerodynamic loads. Assuming similar assumptions to the ones used in the present work, the time needed to set up a new configuration is in principle limited to the extraction of the platform hydrodynamic quantities and the setting up of the geometrical locations of critical reference frames, such as at hub, at fairleads, at tower base, at COG, and at COB. Any quantity that effectively does not affect the preprocessing stage can be parametrized. In order to validate the method, a comparative analysis against fully-coupled aero-hydro-servo-elastic tools is set forth. The comparison is developed in terms of standard IEA LCs, consisting of eigenanalysis, free-decay time series, periodic time series, RAOs, and PSDs. Analysis results show very good agreement between the codes. Furthermore, preliminary performance analysis shows how the new method proposed is significantly faster than the reference code FAST. This simplified method can thus be used as a fast, simplified alternative to study FOWTs concepts of arbitrary shape and configuration. Assumptions employed by the method, however, entail unavoidable limitations. Aerodynamic effects induced by unsteady dynamic motions are neglected, such as dynamic inflow effects and skewed effects. The effect of rotor and drivetrain dynamics on the system dynamics is also neglected, affecting platform yaw dynamics

by the lack of pitch-yaw coupling resulting from rotor gyroscopic effects. Inaccurate yaw response will also most likely influence tension at the mooring lines bridles, which, however, are not considered in the present study. Significant improvement of the present model response may, therefore, be achieved by including the simplified rotor dynamics to the multibody system. The development of BEM aerodynamics capabilities, structural dynamics, complete rotor dynamics in OpenModelica, as well as the expansion, the optimization, and the parametrization of the associated open-source package, will be the subject of future work.

Declaration of competing interest

The authors declare that they have no known competing financial interests or personal relationships that could have appeared to influence the work reported in this paper.

Acknowledgment

This PhD project is financed by the Equinor Akademia program at the University of Stavanger.

References

[1]] Hywind Demo. 2020. equinor.com.
[2]] Wind float. 2020. principlepowerinc.com.
[3] Equinor ASA, Statoil to build the worlds first floating wind farm: Hywind Scotland.
[4] Cruz J, Atcheson M. Floating offshore wind energy - the next generation of wind energy. Springer; 2016.
[5] Jonkman JM. Dynamics modeling and loads analysis of an offshore floating wind turbine. 2007. NREL/TP-500-41958, November.
[6] Jonkman JM. Dynamics of offshore floating wind turbines-model development and verification, vol. 12. Wind Energy; 2009. p. 459–92.
[7] Strobel M, Vorpahl F, Hillmann C, Gu X, Zuga A, Wihlfahrt U. The OnWind Modelica library for offshore wind turbines - implementation and first results. In: Proceedings of the 12th international Modelica conference; 2011. p. 633–42.
[8] Leimeister M, Thomas P. The OneWind Modelica library for floating offshore wind turbine simulations with flexible structures". Proceed. 12th Int. Mod. Conf. 2017:633–42.
[9] Brommundt M, Muskulus M, Strach-Sonsalla M, Strobel M, Vorpahl F. Experiences with object-oriented and equation based modeling of a floating support structure for wind turbines in Modelica". Proceed. Winter Simul. Conf. 2012;1–12.
[10] Modelica Official Website - Modelica Language, 2020.
[11] Elmqvist H. Modelica evolution from my perspective. In: Proceedings of the 10th international ModelicaConference; 2014.
[12] OpenModelica Off. Website 2020.
[13] Jonkman JM. Definition of the floating system for phase IV of OC3" NREL/TP-500-47535. 2010.
[14] Ramachandran GKV, Robertson A, Jonkman JM, Masciola MD. Investigation of response amplitude operators for floating offshore wind turbines" NREL CP-5000-58098. July 2013.
[15] Faltinsen OM. Sea loads on ships and offshore structures". Cambridge Ocean Technology Series; 1993.
[16] Box GEP, Muller ME. A note on the generation of random normal deviates, vol. 29. The Institute of Mathematical Statistics; 1958. p. 610–1. Number 2.
[17]] IEC 61400-3-1:2009" IEC. 2009.
[18] Cummins WE. The impulse response function and ship motions" schiffstechnik 1962;109. 101â€.
[19] Perez T, Fossen TI. Time- vs. Frequency-domain identification of parametric radiation force models for marine structures at zero speed" modeling. Identif. Contr. 2008;29.
[20] Kristiansen E, Egeland O. Frequency-dependent added mass in models for controller design for wave motion damping. IFAC Proceed. Vol. 2003;36(Issue 21): 67–72. ISSN 1474-6670.
[21] Duarte T, Sarmento A, Alves M, Jonkman JM. State-space realization of the wave-radiation force within FAST" NREL. 2013. June.
[22] Kung SY. A new identification and model reduction algorithm via singular value decomposition". Proc. Twelfth Asimolar Conf. Circuit. Syst. Comput. 1978: 70571.
[23] Machowski J, Bialek JW, Bumby JR. Power system dynamics. Stability and control. John Wiley and Sons; 2012.
[24] Kenney C, Hewer G. Necessary and sufficient conditions for balancing unstable systems" automatic control. IEEE Trans. 1987;32:157–60. November.
[25] DNV GL - WADAM Official Website, 2020.
[26] Cruz J, Atcheson M. Floating offshore wind energy: the next generation of wind energy. Springer; 2016.
[27] Karimirad M, Moan T. A simplified method for coupled analysis of floating offshore wind turbines. Mar Struct 2012;27(Issue 1):45–63.
[28] Skaare B, Hanson T, Nielsen F. Integrated dynamic analysis of floating offshore wind turbines" OMAE2006-92291. 2008. p. 671–9.
[29] Jonkman JM, Larsen T, Hansen A, Nygaard T, Maus K, Karimirad M, Gao Z, Moan T, Fylling I, Nichols J, Kohlmeier M, Vergara J, Merino D, Shi W, Park H. Offshore code comparison collaboration within IEA wind Task 23: phase IV results regarding floating wind turbine modeling" European wind energy conference. EWEC); 2010.
[30] Leimeister M, Kolios A, Collu M. Development and verification of an aero-hydro-servo-elastic coupled model of dynamics for FOWT. Based MoWiT Libr. Energies 1974;13:2020. https://doi.org/10.3390/en13081974.
[31] SeaFEM. Analysis of the response amplitude operator (RAO) of a spar buoy wind turbine" Validation. Case 2018;18. November.
[32] Lin YH, Kao SH, Yang CH. Investigation of hydrodynamic forces for floating offshore wind turbines on spar buoys and tension leg platforms with the mooring systems in waves. Applied Sciences; 2019.